Research

Author for correspondence:
Artur L. Gower
e-mail: arturgower@gmail.com

THE ROYAL SOCIETY
PUBLISHING

Reflection from a multi-species material and its transmitted effective wavenumber

Artur L. Gower[1], Michael J. A. Smith[1], William J. Parnell[1] and I. David Abrahams[2]

[1]School of Mathematics, University of Manchester, Oxford Road, Manchester M13 9PL, UK
[2]Isaac Newton Institute for Mathematical Sciences, 20 Clarkson Road, Cambridge CB3 0EH, UK

(iD) ALG, 0000-0002-3229-5451; MJAS, 0000-0001-9514-9438

We formally deduce closed-form expressions for the transmitted effective wavenumber of a material comprising multiple types of inclusions or particles (multi-species), dispersed in a uniform background medium. The expressions, derived here for the first time, are valid for moderate volume fractions and without restriction on the frequency. We show that the multi-species effective wavenumber is not a straightforward extension of expressions for a single species. Comparisons are drawn with state-of-the-art models in acoustics by presenting numerical results for a concrete and a water–oil emulsion in two dimensions. The limit of when one species is much smaller than the other is also discussed and we determine the background medium felt by the larger species in this limit. Surprisingly, we show that the answer is not the intuitive result predicted by self-consistent multiple scattering theories. The derivation presented here applies to the scalar wave equation with cylindrical or spherical inclusions, with any distribution of sizes, densities and wave speeds. The reflection coefficient associated with a halfspace of multi-species cylindrical inclusions is also formally derived.

1. Summary

Materials comprising mixtures of diverse particles, inclusions, defects or inhomogeneities dispersed inside

2

a background medium arise in a wide range of applications, including composite materials, emulsions, gases, polymers, foods and paints. We will refer to these as multi-species materials. Of great importance is the ability to characterize these materials and their *microstructure*, such as particle size distribution and volume fractions. One approach to do this is to employ waves, including electromagnetic, acoustic and elastodynamic waves. If either the receivers are much larger than the inclusions, or the wavelength is much longer than the inclusions, then the receivers will measure the *ensemble-averaged* properties of the wave [1]. This includes the wave speed, attenuation and reflection. Even methods that estimate fluctuations of the wave on smaller scales, such as the averaged intensity, often require the ensemble-averaged wave properties as a first step [2–4]. So in order to improve material characterization, or to design materials with tailored properties, a crucial step is to rigorously calculate the sound speed and attenuation for multi-species materials.

In this paper, we present and formally deduce the effective wavenumber and reflected field of a plane wave scattered by a material comprising different families, or *species*, of particles with distributions of sizes and properties. The work here differs from the existing literature as our results are not limited to low frequencies and are valid for moderate number density. This is achieved by extending the methods introduced in [5] for calculating the effective transmission into a halfspace of a single-species material.

Our approach does not rely on an extinction theorem or the manipulation of divergent integrals or series. The one assumption that is employed is the *quasi-crystalline approximation* [6]. For a single species, this approximation is supported by theoretical [7,8], numerical [9] and experimental [10] evidence; however, the authors are unaware of any rigorous bounds for the error introduced by this approximation. We remark that the quasi-crystalline approximation (QCA) makes no assumption on the material properties, so in principal it is consistent for weak scattering, low or high frequency, or in dense or sparse mixtures. It is also exact when there is only one possible configuration for the particles, for example when the particle centres lie on the coordinates of a crystal lattice (Lax [11], where QCA is discussed under (4.3)). For simplicity, we also restrict attention to the case of circular cylindrical or spherical particles, although our methods can be extended to the case of general-shaped particles by using Waterman's T-matrix approach, e.g. [12–14].

In the context of electromagnetic wave scattering, methods for predicting wave propagation and reflection for multi-species material have previously been developed [3,4,15]. These models have been useful for interpreting data from remote sensing, although it appears that such models cannot systematically reproduce experimental results [16]. In numerous contexts, but particularly in the context of electromagnetics, the standard approach is to employ the Lippman–Schwinger formulation [17,18]. However, such a formulation is restrictive as it is not valid for magnetic media in the electromagnetism context or for scatterers with varying density in acoustics, as identified in [19]. Although it is possible to extend the Lippman–Schwinger formulation to account for this effect [19], we found it simpler to extend the multiple scattering theory [2,20,21].

Our approach is also in contrast to coupled-phase theory where the first step is to estimate the ensemble average of the governing equations [22], without explicitly considering multiple scattering. Although this method can accommodate hydrodynamic interactions and has been extended to polydisperse inclusions (multi-species) it does not completely capture multiple scattering [23,24].

A suggestion for calculating the multi-species effective wavenumber came from Waterman & Truell, eqn (3.25a) in the conclusion of [25]. Their suggested formula has been extensively employed in acoustics, e.g. [26–28]. However, their formula is only valid for low frequency and dilute distributions of particles [21], so it does not properly account for multiple scattering. The approach in [25] combined with [29] led eventually to the state-of-the-art models for the effective acoustic wavenumber in colloidal dispersions [28]. We numerically compare our results with these authors.

Given an overall particle number density $\mathfrak{n}$ and background wavenumber k, our main results for a multi-species material comprising *circular cylinders* are the effective transmitted wavenumber:

$$k_*^2 = k^2 - 4i\mathfrak{n}\,\langle f_\circ \rangle(0) - 4i\mathfrak{n}^2 \langle f_{\circ\circ} \rangle(0) + \mathcal{O}(\mathfrak{n}^3) \tag{1.1}$$

and for an incident wave $u_{\text{in}} = e^{i\alpha x + i\beta y}$, with $(\alpha, \beta) = k(\cos\theta_{\text{in}}, \sin\theta_{\text{in}})$, the averaged reflected wave from the inhomogeneous halfspace,

$$\langle u_{\text{ref}} \rangle = \frac{\mathfrak{n}}{\alpha^2}[R_1 + \mathfrak{n}R_2]\, e^{-i\alpha x + i\beta y} + \mathcal{O}(\mathfrak{n}^3), \tag{1.2}$$

where

$$R_1 = i\langle f_\circ \rangle(\theta_{\text{ref}}), \quad \theta_{\text{ref}} = \pi - 2\theta_{\text{in}}, \tag{1.3}$$

$$R_2 = \frac{2\langle f_\circ \rangle(0)}{\alpha^2}\left[\frac{\alpha\beta}{k^2}\langle f_\circ \rangle'(\theta_{\text{ref}}) - \langle f_\circ \rangle(\theta_{\text{ref}})\right] + i\langle f_{\circ\circ} \rangle(\theta_{\text{ref}}) \tag{1.4}$$

and the functions $\langle f_\circ \rangle$ and $\langle f_{\circ\circ} \rangle$ are defined in (4.12) and (4.13). The formula (1.2) is briefly deduced in §7a, and in figure 7 we give a pictorial representation, although we stress that the choice $\theta_{\text{ref}} = \pi - 2\theta_{\text{in}}$ is not due to a simple geometric argument, but appears from rigorous derivations. From the reflection coefficient (1.2), it is possible to choose effective material properties [30]. However, because the reflection coefficient depends on the angle of incidence via $\langle f_\circ \rangle(\theta_{\text{ref}})$ and $\langle f_{\circ\circ} \rangle(\theta_{\text{ref}})$, it is likely that these effective material properties change with the angle of incidence.

In the electronic supplementary material, we provide a brief self-contained version of these formulae, and the corresponding result for spherical particles, both for a finite number of species. We also provide open source code that implements these formulae [31]. For spherical inclusions, the effective transmitted acoustic wavenumber becomes

$$k_*^2 = k^2 - \mathfrak{n}\frac{4\pi i}{k}\langle F_\circ \rangle(0) + \mathfrak{n}^2\frac{(4\pi)^2}{k^4}\langle F_{\circ\circ} \rangle + \mathcal{O}(\mathfrak{n}^3), \tag{1.5}$$

where $\langle F_\circ \rangle$ and $\langle F_{\circ\circ} \rangle$ are functions associated with scattering from the spherical particle and are defined in (A 2). Note that $\langle F_{\circ\circ} \rangle$ has no θ dependency. For a longer discussion of multiple scattering from spheres, see [30].

By developing *multi-species* formulae valid for higher number densities and frequencies, we open up the possibility of characterizing and designing a wide range of advanced materials. The effects of multiple scattering appear only for moderate number density, i.e. in the term $\langle f_{\circ\circ} \rangle(0)$ in (1.1) and $\langle F_{\circ\circ} \rangle$ in (1.5). One important consequence of this multiple scattering term is that a multi-species material can exhibit properties not exhibited by that of the background medium with only one constituent species. We stress that even for just two types of circular cylindrical particles, the effects of multiple scattering are neither intuitive nor easily deduced from the single-species case. This becomes apparent in the simple example of a multi-species material where one species is much smaller than the other. In this scenario, we compare our expression for the multi-species effective wavenumber with the state-of-the-art models from acoustics [28] and a *self-consistent* type approximation [32–34], which can be calculated from the single-species formula via an iterative approach: first one *homogenizes* the small particle and background mixture before considering the multiple scattering of the larger particles in the new (homogenized) background medium. We show analytically that this naive self-consistent methodology is not even correct in the low-frequency limit. This is then demonstrated numerically for the cases of an emulsion and concrete. Our results are in in-line with [35], who discuss an effective medium model of a three-phased material in the low-frequency limit.

The outline of this paper is as follows. In §2, we describe the exact theory of multiple scattering for N cylinders of any radius, density and sound speed. From there we calculate the effective (ensemble-averaged) equations and apply statistical approximations in §3. In §4, we deduce the governing system for the effective wavenumbers at arbitrary total number density and arbitrary frequency, before specializing the result to the case of moderate number fraction and

low frequency. In §5, we investigate the specific, representative case of two types of circular cylindrical species and compare different approximations graphically. To calculate the reflected or transmitted wave we also need the effective amplitude, which we calculate in §7 followed by the effective reflected wave. We close in §8, where we discuss avenues for improvement of the techniques and more general further work.

2. Multipole method for cylinders

In this section, we describe the exact theory for scalar multiple wave scattering from a finite number N of circular cylinders possessing different densities, wave speeds and radii. Parameters associated with the medium are summarized in table 1. Naturally, the system of equations describing this problem bears strong similarities to that obtained by Záviška (see references in [36] and in [5] for the single species circular cylindrical particle context). Assuming time-harmonic dependence of the form $e^{-i\omega t}$, the pressure u outside all the cylinders satisfies the scalar Helmholtz equation

$$\nabla^2 u + k^2 u = 0 \qquad (2.1a)$$

and inside the jth cylinder the pressure u_j satisfies

$$\nabla^2 u_j + k_j^2 u_j = 0, \quad \text{for } j = 1, 2, \ldots, N, \qquad (2.1b)$$

where ∇^2 is the two-dimensional Laplacian and

$$k = \frac{\omega}{c} \quad \text{and} \quad k_j = \frac{\omega}{c_j}. \qquad (2.2)$$

We consider an incident plane wave

$$u_{\text{in}}(x, y) = e^{i(\alpha x + \beta y)}, \quad \text{with } (\alpha, \beta) = k(\cos\theta_{\text{in}}, \sin\theta_{\text{in}})$$

and use for each cylinder the polar coordinates

$$R_j = \|\mathbf{x} - \mathbf{x}_j\|, \quad \Theta_j = \arctan\left(\frac{y - y_j}{x - x_j}\right), \qquad (2.3)$$

where $\mathbf{x}_j$ is the centre of the jth cylinder and $\mathbf{x} = (x, y)$ is an arbitrary point with origin O. (See figure 1 for a schematic of the material properties and coordinate systems.) Then we can define u_j as the scattered pressure field from the jth cylinder,

$$u_j(R_j, \Theta_j) = \sum_{m=-\infty}^{\infty} A_j^m Z_j^m H_m(kR_j) e^{im\Theta_j}, \quad \text{for } R_j > a_j, \qquad (2.4)$$

where H_m are Hankel functions of the first kind, A_j^m are arbitrary coefficients and Z_j^m characterizes the type of scatterer:

$$Z_j^m = \frac{q_j J_m'(ka_j) J_m(k_j a_j) - J_m(ka_j) J_m'(k_j a_j)}{q_j H_m'(ka_j) J_m(k_j a_j) - H_m(ka_j) J_m'(k_j a_j)} = Z_j^{-m}, \qquad (2.5)$$

with $q_j = (\rho_j c_j)/(\rho c)$. In the limits $q_j \to 0$ or $q_j \to \infty$, the coefficients for Dirichlet or Neumann boundary conditions are recovered, respectively.

The pressure outside all cylinders is the sum of the incident wave u_{in} and all scattered waves,

$$u(x, y) = u_{\text{in}}(x, y) + \sum_{j=1}^{N} u_j(R_j, \Theta_j) \qquad (2.6)$$

and the total field inside the jth cylinder is

$$u_j^{\text{I}}(R_j, \Theta_j) = \sum_{m=-\infty}^{\infty} B_j^m J_m(k_j R_j) e^{im\Theta_j}, \quad \text{for } R_j < a_j. \qquad (2.7)$$
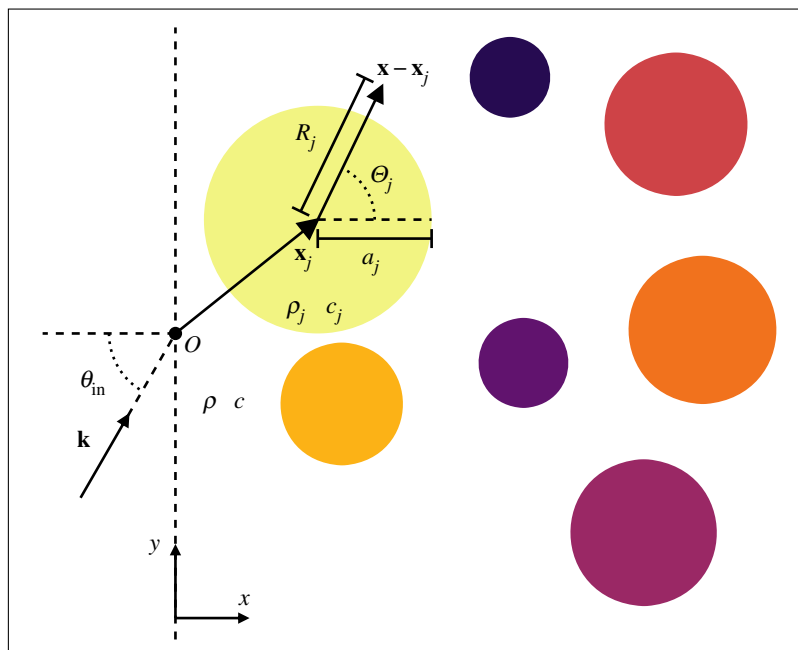
Figure 1. Represents a multi-species material comprising different species of cylinders to the right of the origin $O = (0, 0)$. The vector $\mathbf{x}_j$ points to the centre of the jth cylinder, with a local polar coordinate system (R_j, Θ_j). Each cylinder has a radius a_j, density ρ_j and wave speed c_j, while the background has density ρ and wave speed c. The vector $\mathbf{k}$ is the direction of the incident plane wave. (Online version in colour.)

Table 1. Summary of material properties and notation. The index j refers to properties of the jth species, see figure 1 for an illustration.

background properties:		density ρ	sound speed c	
species properties:	number density n_j	density ρ_j	sound speed c_j	radius a_j

In the above, J_m are Bessel functions of the first kind. The arbitrary constants A_j^m and B_j^m in (2.4) and (2.7) will be determined from the boundary conditions of the jth cylinder $R_j = a_j$. The boundary conditions of continuity of pressure and normal velocity on the cylinder boundaries are given, respectively, by

$$u = u_j^{\mathrm{I}} \quad \text{and} \quad \frac{1}{\rho} \frac{\partial u}{\partial R_j} = \frac{1}{\rho_j} \frac{\partial u_j^{\mathrm{I}}}{\partial R_j}, \quad \text{on } R_j = a_j \quad \text{for } j = 1, \dots, N, \tag{2.8}$$

recalling that ρ and ρ_j denote the material densities of the background and of the jth cylinder respectively. To impose the boundary conditions, we now express the relevant fields in terms of the (R_j, Θ_j) coordinate system. For the incident wave

$$u_{\mathrm{in}}(x, y) = I_j \, \mathrm{e}^{\mathrm{i}kr_j \cos(\theta_j - \theta_{\mathrm{in}})} = I_j \sum_{n=-\infty}^{\infty} \mathrm{e}^{\mathrm{i}n(\pi/2 - \Theta_j + \theta_{\mathrm{in}})} J_n(kR_j), \tag{2.9}$$

where $I_j = u_{\mathrm{in}}(x_j, y_j)$ following the Jacobi–Anger expansion [37]. For the scattered waves (2.4), we use Graf's addition theorem (9.1.79) in [38],

$$H_n(kR_\ell) \, \mathrm{e}^{\mathrm{i}n\Theta_\ell} = \sum_{m=-\infty}^{\infty} H_{n-m}(kR_{\ell j}) \, \mathrm{e}^{\mathrm{i}(n-m)\Theta_{\ell j}} J_m(kR_j) \, \mathrm{e}^{\mathrm{i}m\Theta_j}, \quad \text{for } R_j < R_{\ell j}, \tag{2.10}$$

where $(R_{\ell j}, \Theta_{\ell j})$ is the polar form of the vector $\mathbf{x}^j - \mathbf{x}^\ell$. Using the above and (2.9) we can impose the boundary conditions (2.8) to arrive at the following system of equations

$$A_j^m + I_j\,\mathrm{e}^{\mathrm{i}m(\pi/2-\theta_{\mathrm{in}})} + \sum_{n=-\infty}^{\infty}\sum_{\substack{\ell=1\\\ell\neq j}}^{N} A_\ell^n Z_\ell^n\,\mathrm{e}^{\mathrm{i}(n-m)\Theta_{\ell j}} H_{n-m}(kR_{\ell j}) = 0, \tag{2.11}$$

for $j = 1, \ldots, N$ and all integers m. Furthermore, the coefficients associated with the pressure inside the cylinder (2.7) are then given by

$$B_j^m = \frac{A_j^m}{J_m(k_j a_j)}[Z_j^m H_m(ka_j) - J_m(ka_j)] \tag{2.12}$$

and subsequently, the field $u(x,y)$ is entirely prescribed.

In any given material, it is impossible to know the exact position and properties of all constituent particles. Our goal is, therefore, to solve (2.11) not for one particular configuration of scatterers, but instead to calculate the average value of the coefficients A_j^m, denoted by $\langle A_j^m \rangle$, from which we can calculate an effective wavenumber and reflection. Note that the *effective* field describes the *ensemble-averaged* field that is usually measured in an acoustic experiment, as the receiver face is typically much larger than the particles and the distance between them [1,39]. In our case, we obtain an ensemble average by averaging over all particle configurations and all the material properties of the particles. This approach is general and can be tailored to different scenarios, e.g. when detailed information *is* known about the particle material properties.

3. Averaged multiple scattering

For an introduction to ensemble averaging of multiple scattering, see [2,40], where the result for a classical dilute isotropic mixture was determined. Here we present a brief self-contained explanation tailored to multi-species.

Consider a configuration of N circular cylinders centred at $\mathbf{x}_1, \mathbf{x}_2, \ldots, \mathbf{x}_N$ with the scattering properties $\mathbf{s}_1, \mathbf{s}_2, \ldots, \mathbf{s}_N$, where $\mathbf{s}_j$ denotes the properties of the jth cylinder, i.e. here these are $\mathbf{s}_j = (a_j, \rho_j, c_j)$. Each $\mathbf{x}_j$ is in the region $\mathcal{R}_N$, where $\mathfrak{n} = N/|\mathcal{R}_N|$ is the total number density and $|\mathcal{R}_N|$ is the area of $\mathcal{R}_N$. The properties $\mathbf{s}_j$ are taken from the set $\mathcal{S}$. For example, we could have $\mathcal{S} = [0,1] \times [1,2] \times [100,200]$, so that $a_j \in [0,1]$, $\rho_j \in [1,2]$ and $c_j \in [100,200]$.

The probability of the cylinders being in a specific configuration is given by the probability density function $p(\{\mathbf{x}_1, \mathbf{s}_1\}, \{\mathbf{x}_2, \mathbf{s}_2\}, \ldots, \{\mathbf{x}_N, \mathbf{s}_N\})$. Using the compact notation $\Lambda_i = \{\mathbf{x}_i, \mathbf{s}_i\}$ to denote the properties of the i-th cylinder, it follows that

$$\int p(\Lambda_1)\,\mathrm{d}\Lambda_1 = \iint p(\Lambda_1, \Lambda_2)\,\mathrm{d}\Lambda_1\,\mathrm{d}\Lambda_2 = \cdots = 1, \tag{3.1}$$

where each integral is taken over *both* $\mathcal{R}_N$ (for $\mathbf{x}_j$) and $\mathcal{S}$ (for $\mathbf{s}_j$) with $\mathrm{d}\Lambda_j = \mathrm{d}\mathbf{x}_i\,\mathrm{d}\mathbf{s}_i$. Note that $p(\Lambda_1, \Lambda_2)$ is the probability of one cylinder having the properties Λ_1 and another having the properties Λ_2, when the properties of all the remaining $N - 2$ cylinders are unknown. And as the cylinders are indistinguishable: $p(\Lambda_1, \Lambda_2) = p(\Lambda_2, \Lambda_1)$. Furthermore, we have

$$p(\Lambda_1, \ldots, \Lambda_N) = p(\Lambda_j)p(\Lambda_1, \ldots, \Lambda_N \mid \Lambda_j) \tag{3.2a}$$

and

$$p(\Lambda_1, \ldots, \Lambda_N \mid \Lambda_j) = p(\Lambda_\ell \mid \Lambda_j)p(\Lambda_1, \ldots, \Lambda_N \mid \Lambda_\ell, \Lambda_j), \tag{3.2b}$$

where $p(\Lambda_1, \ldots, \Lambda_N \mid \Lambda_j)$ is the conditional probability of having cylinders with the properties $\Lambda_1, \ldots, \Lambda_N$ (not including Λ_j), given that the jth cylinder has the properties Λ_j. Likewise, $p(\Lambda_1, \ldots, \Lambda_N \mid \Lambda_\ell, \Lambda_j)$ is the conditional probability of having cylinders with the properties $\Lambda_1, \ldots, \Lambda_N$ (not including Λ_ℓ and Λ_j) given that there are already two cylinders present, with properties Λ_ℓ and Λ_j.

Given some function $F(\boldsymbol{\Lambda}_1, \ldots, \boldsymbol{\Lambda}_N)$, we denote its average, or *expected value*, by

$$\langle F \rangle = \int \cdots \int F(\boldsymbol{\Lambda}_1, \ldots, \boldsymbol{\Lambda}_N) p(\boldsymbol{\Lambda}_1, \ldots, \boldsymbol{\Lambda}_N) \, \mathrm{d}\boldsymbol{\Lambda}_1 \ldots \mathrm{d}\boldsymbol{\Lambda}_N. \tag{3.3}$$

If we fix the location and properties of the jth cylinder, $\boldsymbol{\Lambda}_j$ and average over all the properties of the other cylinders, we obtain a *conditional average* of F given by

$$\langle F \rangle_{\boldsymbol{\Lambda}_j} = \int \cdots \int F(\boldsymbol{\Lambda}_1, \ldots, \boldsymbol{\Lambda}_N) p(\boldsymbol{\Lambda}_1, \ldots, \boldsymbol{\Lambda}_N \mid \boldsymbol{\Lambda}_j) \, \mathrm{d}\boldsymbol{\Lambda}_1 \ldots \boldsymbol{\Lambda}_N, \tag{3.4}$$

where we do not integrate over $\boldsymbol{\Lambda}_j$. The average and conditional averages are related by

$$\langle F \rangle = \int \langle F \rangle_{\boldsymbol{\Lambda}_j} p(\boldsymbol{\Lambda}_j) \, \mathrm{d}\boldsymbol{\Lambda}_j \quad \text{and} \quad \langle F \rangle_{\boldsymbol{\Lambda}_j} = \int \langle F \rangle_{\boldsymbol{\Lambda}_j \boldsymbol{\Lambda}_\ell} p(\boldsymbol{\Lambda}_\ell) \, \mathrm{d}\boldsymbol{\Lambda}_\ell, \tag{3.5}$$

where $\langle F \rangle_{\boldsymbol{\Lambda}_\ell \boldsymbol{\Lambda}_j}$ is the conditional average when fixing both $\boldsymbol{\Lambda}_j$ and $\boldsymbol{\Lambda}_\ell$, and $\langle F \rangle_{\boldsymbol{\Lambda}_\ell \boldsymbol{\Lambda}_j} = \langle F \rangle_{\boldsymbol{\Lambda}_j \boldsymbol{\Lambda}_\ell}$.

Returning to the task of obtaining effective properties for a multi-species medium, we multiply the system (2.11) by $p(\boldsymbol{\Lambda}_2, \ldots, \boldsymbol{\Lambda}_N \mid \boldsymbol{\Lambda}_1)$ and average over $\boldsymbol{\Lambda}_2, \ldots, \boldsymbol{\Lambda}_N$, to reach

$$\sum_{n=-\infty}^{\infty} \sum_{\ell=2}^{N} \int \langle A_\ell^n \rangle_{\boldsymbol{\Lambda}_\ell \boldsymbol{\Lambda}_1} Z^n(\mathbf{s}_\ell) \, \mathrm{e}^{\mathrm{i}(n-m)\Theta_{\ell 1}} H_{n-m}(kR_{\ell 1}) p(\boldsymbol{\Lambda}_\ell \mid \boldsymbol{\Lambda}_1) \, \mathrm{d}\boldsymbol{\Lambda}_\ell$$
$$+ \langle A_1^m \rangle_{\boldsymbol{\Lambda}_1} + I_1 \, \mathrm{e}^{\mathrm{i}m(\pi/2-\theta_{\mathrm{in}})} = 0,$$

where, without loss of generality, we have chosen $j=1$, used the conditional average definition (3.2*b*) and defined $Z^n(\mathbf{s}_\ell) := Z_\ell^n$ to make the dependency on $\mathbf{s}_\ell$ explicit. To further simplify the above, note that all terms in the sum over ℓ give the same value. That is, the terms in the integrand depend on ℓ solely through the dummy variable $\boldsymbol{\Lambda}_\ell$. In particular, the probability distribution is the same for each cylinder, and if $\boldsymbol{\Lambda}_2 = \boldsymbol{\Lambda}_l$, then $\langle A_\ell^n \rangle_{\boldsymbol{\Lambda}_\ell \boldsymbol{\Lambda}_1} = \langle A_2^n \rangle_{\boldsymbol{\Lambda}_2 \boldsymbol{\Lambda}_1}$, because equation (2.11) uniquely determines the coefficients A_ℓ^n from the position and scattering properties $\boldsymbol{\Lambda}_\ell$. We use this to obtain

$$\sum_{n=-\infty}^{\infty} (N-1) \int \langle A_2^n \rangle_{\boldsymbol{\Lambda}_2 \boldsymbol{\Lambda}_1} Z^n(\mathbf{s}_2) \, \mathrm{e}^{\mathrm{i}(n-m)\Theta_{21}} H_{n-m}(kR_{21}) p(\boldsymbol{\Lambda}_2 \mid \boldsymbol{\Lambda}_1) \, \mathrm{d}\boldsymbol{\Lambda}_2$$
$$+ \langle A_1^m \rangle_{\boldsymbol{\Lambda}_1} + I_1 \, \mathrm{e}^{\mathrm{i}m(\pi/2-\theta_{\mathrm{in}})} = 0. \tag{3.6}$$

Our aim is to solve the system above for $\langle A_1^m \rangle_{\boldsymbol{\Lambda}_1}$; however, this requires that we make assumptions about $p(\boldsymbol{\Lambda}_2 \mid \boldsymbol{\Lambda}_1)$ and $\langle A_2^n \rangle_{\boldsymbol{\Lambda}_2, \boldsymbol{\Lambda}_1}$. These approximations are discussed in §3a; however, for the moment, we assume that an appropriate substitution has been imposed.

With $\langle A_1^m \rangle_{\boldsymbol{\Lambda}_1}$, we can calculate the average total pressure (incident plus scattered), measured at some position $\mathbf{x}$ outside $\mathcal{R}_N$, by averaging (2.6) to obtain

$$\langle u(x,y) \rangle = u_{\mathrm{in}}(x,y) + \sum_{j=1}^{N} \int \cdots \int u_j(R_j, \Theta_j) p(\boldsymbol{\Lambda}_1, \ldots, \boldsymbol{\Lambda}_N) \, \mathrm{d}\boldsymbol{\Lambda}_1 \ldots \mathrm{d}\boldsymbol{\Lambda}_N, \tag{3.7}$$

where $\langle u_{\mathrm{in}}(x,y) \rangle = u_{\mathrm{in}}(x,y)$ because the incident field is independent of the scattering configuration. We can then rewrite the average outgoing wave u_j by fixing the properties of the jth cylinder $\boldsymbol{\Lambda}_j$ and using equation (3.2*a*) to reach

$$\langle u(x,y) \rangle - u_{\mathrm{in}}(x,y) = \sum_{j=1}^{N} \int \langle u_j(R_j, \Theta_j) \rangle_{\boldsymbol{\Lambda}_j} p(\boldsymbol{\Lambda}_j) \, \mathrm{d}\boldsymbol{\Lambda}_j = N \int \langle u_1(R_1, \Theta_1) \rangle_{\boldsymbol{\Lambda}_1} p(\boldsymbol{\Lambda}_1) \, \mathrm{d}\boldsymbol{\Lambda}_1. \tag{3.8}$$

Likewise, for the conditionally averaged scattered field (2.4) measured at $\mathbf{x}$, we obtain

$$\langle u_1(R_1, \Theta_1) \rangle_{\boldsymbol{\Lambda}_1} = \sum_{m=-\infty}^{\infty} \langle A_1^m \rangle_{\boldsymbol{\Lambda}_1} Z^m(\mathbf{s}_1) H_m^{(1)}(kR_1) \, \mathrm{e}^{\mathrm{i}m\Theta_1}. \tag{3.9}$$

We use the above to calculate the reflection from a halfspace in §7a and to obtain (1.2). To proceed we need to solve the system (3.6) and, in line with existing approaches, we do this by making statistical approximations.

(a) Statistical approximations

In order to solve (3.6) for $\langle A_1^n \rangle_{\Lambda_1}$, we need an approximation for $\langle A_2^n \rangle_{\Lambda_2,\Lambda_1}$ and the pair distribution $p(\Lambda_2 \mid \Lambda_1)$. In this work, we adopt the standard *closure* approximation for single species, but extended to multi-species, the QCA [5,6]:

$$\langle A_2^n \rangle_{\Lambda_2 \Lambda_1} \approx \langle A_2^n \rangle_{\Lambda_2}. \tag{3.10}$$

This approximation still makes sense for multi-species because it replaces the dependence of $\langle A_2^n \rangle_{\Lambda_2,\Lambda_1}$ in Λ_1 by its expected value in Λ_1. Note also that the expected difference in Λ_2:

$$\int [\langle A_2^n \rangle_{\Lambda_2 \Lambda_1} - \langle A_2^n \rangle_{\Lambda_2}] p(\Lambda_2) \, d\Lambda_2 = \langle A_2^n \rangle_{\Lambda_1} - \langle A_2^n \rangle \approx 0,$$

for a large number of scatterers.

Using QCA, we introduce the notation

$$\mathcal{A}^n(\mathbf{x}_j, \mathbf{s}_j) = \langle A_j^n \rangle_{\Lambda_j} \quad \text{and} \quad \mathcal{A}^n(\mathbf{x}_j, \mathbf{s}_j) = \langle A_j^n \rangle_{\Lambda_j \Lambda_k}, \quad \text{for } k \neq j. \tag{3.11}$$

Next, we determine a suitable approximation for the pair distribution $p(\Lambda_2 | \Lambda_1)$, beginning with (3.2a) to write

$$p(\Lambda_2 \mid \Lambda_1) = [p(\Lambda_1)]^{-1} p(\Lambda_1, \Lambda_2). \tag{3.12}$$

For clarity, we introduce the spatial random variables $\mathbf{X}_1, \mathbf{X}_1, \ldots, \mathbf{X}_N$ and the scattering property random variables $\mathbf{S}_1, \mathbf{S}_1, \ldots, \mathbf{S}_N$, and write probability density functions in the form, e.g.

$$p(\Lambda_1, \ldots, \Lambda_N) = P(\mathbf{X}_1 = \mathbf{x}_1, \ldots, \mathbf{X}_N = \mathbf{x}_N, \mathbf{S}_1 = \mathbf{s}_1, \ldots, \mathbf{S}_N = \mathbf{s}_N). \tag{3.13}$$

In the first instance, we assume the random uniform distribution

$$p(\Lambda_1) = \frac{1}{|\mathcal{R}_N|} P(\mathbf{S}_1 = \mathbf{s}_1), \tag{3.14}$$

where $P(\mathbf{S}_1 = \mathbf{s}_1)$ is the probability density in $\mathcal{S}$ that the particle will have scattering property $\mathbf{s}_1$. The above assumes that $P(\mathbf{X}_1 = \mathbf{x}_1 \mid \mathbf{S}_1 = \mathbf{s}_1) = |\mathcal{R}_N|^{-1}$, i.e. that the position $\mathbf{x}_1$ of the cylinder is independent of the scattering property $\mathbf{s}_1$. This is not always the case, for example, depending on the size of the cylinder, some positions near the boundary of $\mathcal{R}_N$ may be infeasible. However, these boundary effects are negligible when taking the limit $|\mathcal{R}_N| \to \infty$.

For the remaining distribution in (3.12), we use

$$p(\Lambda_1, \Lambda_2) = P(\mathbf{S}_1 = \mathbf{s}_1, \mathbf{S}_2 = \mathbf{s}_2) P(\mathbf{X}_1 = \mathbf{x}_1, \mathbf{X}_2 = \mathbf{x}_2 \mid \mathbf{S}_1 = \mathbf{s}_1, \mathbf{S}_2 = \mathbf{s}_2), \tag{3.15}$$

followed by

$$P(\mathbf{S}_1 = \mathbf{s}_1, \mathbf{S}_2 = \mathbf{s}_2) = P(\mathbf{S}_1 = \mathbf{s}_1) P(\mathbf{S}_2 = \mathbf{s}_2), \tag{3.16}$$

which assumes that the scattering properties are statistically independent. Next, we assume that the cylinders are equally likely to be anywhere but do not overlap (a *hole correction* correlation [20]), to write

$$P(\mathbf{X}_1 = \mathbf{x}_1, \mathbf{X}_2 = \mathbf{x}_2 \mid \mathbf{S}_1 = \mathbf{s}_1, \mathbf{S}_2 = \mathbf{s}_2) = \begin{cases} 0 & \text{if } R_{21} \leq a_{21}, \\ |\mathcal{R}_N|^{-2} & \text{if } R_{21} > a_{21}, \end{cases} \tag{3.17}$$

where $R_{21} := \|\mathbf{x}_1 - \mathbf{x}_2\|$, $a_{21} = b_1 + b_2$ for some $b_1 \geq a_1$ and some $b_2 \geq a_2$, and b_1 is the radius of exclusion around $\mathbf{x}_1$ which is usually chosen to be proportional to the radius a_1. Note that when integrating (3.17) above in $\mathbf{x}_1$ and $\mathbf{x}_2$, we obtain $|\mathcal{R}_N|^{-2}(|\mathcal{R}_N|^2 - \pi a_{21}^2) \approx 1$ for $\mathcal{R}_N \gg a_{21}^2$.

Ultimately, substituting (3.16) and (3.17) into (3.15) in tandem with (3.14) leads to the pair distribution

$$p(\Lambda_2 \mid \Lambda_1) = \frac{1}{|\mathcal{R}_N|} p(\mathbf{s}_2) H(R_{21} - a_{21}),$$ (3.18)

where $H(x)$ denotes the Heaviside function, under the assumption $|\mathcal{R}_N| \gg a_{21}^2$. In the next section, we will the approximations (3.11) and (3.18) to solve the system in (3.6) for $\langle A_1^n \rangle_{\Lambda_1}$.

We now include a discussion of other commonly used pair distributions. We remark that for densely packed scatterers, other pair distributions [41] are preferred and take the form

$$P(\mathbf{X}_1 = \mathbf{x}_1, \mathbf{X}_2 = \mathbf{x}_2 \mid \mathbf{S}_1 = \mathbf{s}_1, \mathbf{S}_2 = \mathbf{s}_2) = \begin{cases} 0 & \text{if } R_{21} \leq a_{21}, \\ \dfrac{1 + \chi(R_{21} \mid \mathbf{s}_1, \mathbf{s}_2)}{|\mathcal{R}_N|^2} & \text{if } R_{21} > a_{21}, \end{cases}$$ (3.19)

where

$$\int_{\mathcal{R}_N} \int_{\mathcal{R}_N} \chi(R_{21} \mid \mathbf{s}_1, \mathbf{s}_2) \, d\mathbf{x}_1 \, d\mathbf{x}_2 = 0.$$ (3.20)

To calculate the effective wavenumber for the pair-correlation (3.19), a common choice is to assume that the scatterers are uniformly randomly distributed, which leads to

$$\chi(R_{21} \mid \mathbf{s}_1, \mathbf{s}_2) \approx 0 \quad \text{for } R_{21} > \bar{a}_{21} > 2a_{21},$$ (3.21)

used by Linton & Martin [5, Section D], [42], [43, eqn (27)], where $\bar{a}_{21}$ is some distance large enough for the scatterers at $\mathbf{x}_1$ and $\mathbf{x}_2$ to no longer effect each other. One popular choice for χ is the Percus–Yevick function, which assumes all scatterers are uniformly randomly distributed [44], though χ can also be used to specify if some species are more likely to be closer or further apart.

In this work, we set $\chi = 0$ for simplicity (unless otherwise stated), but also because it is not clear that the error introduced by using $\chi = 0$ is in any way greater than the error committed due to QCA (3.10). Both the hole correction (3.17) and QCA (3.10) make similar assumptions: for $R_{21} > a_{21}$, the hole correction replaces $p(\Lambda_2 \mid \Lambda_1)$ with its expected value in Λ_1:

$$p(\Lambda_2 \mid \Lambda_1) \approx \int p(\Lambda_2 \mid \Lambda_1) p(\Lambda_1) \, d\Lambda_1 = p(\Lambda_2),$$

just as QCA (3.10) assumes that $\langle A_2^n \rangle_{\Lambda_2 \Lambda_1} \approx \langle A_2^n \rangle_{\Lambda_2}$. Similarly for $R_{21} \leq a_{21}$ we would set both $p(\Lambda_2 \mid \Lambda_1) = 0$ and $\langle A_2^n \rangle_{\Lambda_2 \Lambda_1} = 0$ for QCA and hole correction. Another reason to set $\chi = 0$ is because we are interested in the limit for small $\mathfrak{n}$. In this limit, it is expected that $\chi \to 0$ when $\mathfrak{n} \to 0$ for uniformly distributed scatterers, which in turn indicates that the contribution of χ to the effective wave is smaller than $\mathfrak{n}^2$ [5,45].

(b) Infinitely many cylinders in the halfspace

In preceding sections, we considered a finite number of scatterers in a bounded domain $\mathcal{R}_N$. Now we consider the limit $N \to \infty$ and where the region $\mathcal{R}_N$ tends to the halfspace $x > 0$. We will follow [5] and limit the cylinders to the halfspace $x > 0$, as it allows us to avoid divergent integrals, such as those in [46], e.g. between their eqn (32) and (33).

Substituting the approximations (3.18) and (3.11) into the governing system (3.6) leads to

$$\frac{N-1}{|\mathcal{R}_N|} \sum_{n=-\infty}^{\infty} \int_{\mathcal{S}} \int_{\substack{\mathcal{R}_N \\ R_{21} > a_{21}}} \mathcal{A}^n(\mathbf{x}_2, \mathbf{s}_2) \, e^{i(n-m)\Theta_{21}} H_{n-m}(kR_{21}) \, d\mathbf{x}_2 \, d\mathbf{s}_2^n$$

$$+ \mathcal{A}^m(\mathbf{x}_1, \mathbf{s}_1) + I_1 \, e^{im(\pi/2 - \theta_{in})} = 0, \quad \text{for } x_1 > 0,$$ (3.22)

where for brevity, we write

$$d\mathbf{s}_2^n = Z^n(\mathbf{s}_2) p(\mathbf{s}_2) \, d\mathbf{s}_2,$$ (3.23)

with $p(\mathbf{s}_2) = P(\mathbf{S}_2 = \mathbf{s}_2)$. By taking the limits $N \to \infty$ and $\lim_{N \to \infty} \mathcal{R}_N = \{(x_1, x_2) : x_2 > 0\}$, while fixing the number density $\mathfrak{n} = N/|\mathcal{R}_N|$, equation (3.22) takes the form

$$\mathfrak{n} \sum_{n=-\infty}^{\infty} \int_{\mathcal{S}} \int_{\substack{x_2>0 \\ R_{21}>a_{21}}} \mathcal{A}^n(\mathbf{x}_2, \mathbf{s}_2) \, e^{i(n-m)\Theta_{21}} H_{n-m}(kR_{21}) \, dx_2 \, d\mathbf{s}_2^n$$

$$+ \mathcal{A}^m(\mathbf{x}_1, \mathbf{s}_1) + I_1 \, e^{im(\pi/2 - \theta_{in})} = 0, \quad \text{for } x_1 > 0, \tag{3.24}$$

which represents the governing system for our semi-infinite multiple-species problem.

Incidentally, when all cylinders are identical this system reduces to eqn (54) in [5], that is when $p(\mathbf{s}_2) = \delta(a_2 - a)\delta(c_2 - c)\delta(\rho_2 - \rho)$ in (3.23), where $\delta(x)$ represents Dirac's delta function.

4. Effective wavenumber

To solve the system (3.24), first we use the symmetry of the problem to rewrite

$$\mathcal{A}^m(x, y, \mathbf{s}) = \mathcal{A}^m(x, 0, \mathbf{s}) \, e^{i\beta y}, \tag{4.1}$$

that is, if $\mathcal{A}^m$ is a solution to (3.24), then so is $\mathcal{A}_0^m$ defined by $\mathcal{A}_0^m(x, y, \mathbf{s}) = \mathcal{A}^m(x, y - y', \mathbf{s}) \, e^{i\beta y'}$ for every y', then taking $y' = y$ we see that (4.1) is also a solution, recalling that $I_1 = e^{i\alpha x + i\beta y}$ and

$$\alpha = k \cos\theta_{in} \quad \text{and} \quad \beta = k \sin\theta_{in}. \tag{4.2}$$

Sufficiently far away from the boundary, say $x > \bar{x}$, we assume a plane wave ansatz

$$\mathcal{A}^m(x, y, \mathbf{s}) = i^m \, e^{-im\theta_*} \mathcal{A}_*^m(\mathbf{s}) \, e^{i\mathbf{k}_* \cdot \mathbf{x}}, \quad \text{for } x > \bar{x}, \tag{4.3}$$

where the factor $i^m \, e^{-im\theta_*}$ is introduced for later convenience. We could have for generality considered a sum of plane waves, but for low number density this is unnecessary, as we would find a unique $\mathbf{k}_*$ for a halfspace.

Equating (4.1) and (4.3), for $x > \bar{x}$, we obtain Snell's Law

$$k_* \sin\theta_* = k \sin\theta_{in} \quad \text{with} \quad \mathbf{k}_* = (\alpha_*, \beta) := k_*(\cos\theta_*, \sin\theta_*), \tag{4.4}$$

noting that both θ_* and k_* are complex numbers. We also require that $\text{Im}\,\alpha_* > 0$, so that the integral over $\mathbf{x}_2$ in (3.24) converges.

In appendix B, we present the derivation for the system below, which is obtained by substituting (4.1) and (4.3) into (3.24). In the process we establish that $k_* \neq k$, and find that there is no restriction on the length $\bar{x}$, a fact we use to calculate the reflected wave. The result is that (3.24) reduces to the system

$$\mathcal{A}_*^m(\mathbf{s}_1) + 2\mathfrak{n}\pi \sum_{n=-\infty}^{\infty} \int_{\mathcal{S}} \mathcal{A}_*^n(\mathbf{s}_2) \left[\frac{\mathcal{N}_{n-m}(ka_{12}, k_*a_{12})}{k^2 - k_*^2} + \mathcal{X}_* \right] d\mathbf{s}_2^n = 0 \tag{4.5}$$

and

$$\sum_{n=-\infty}^{\infty} e^{in(\theta_{in} - \theta_*)} \int_{\mathcal{S}} \mathcal{A}_*^n(\mathbf{s}_2) \, d\mathbf{s}_2^n = e^{i(\alpha - \alpha_*)\bar{x}}(\alpha_* - \alpha) \left[\frac{\alpha i}{2\mathfrak{n}} + b(\bar{x}) \right], \tag{4.6}$$

in terms of the unknown parameters $\mathcal{A}_*^n(\mathbf{s}_2)$ and k_*, where

$$b(\bar{x}) = (-i)^{n-1} \sum_{n=-\infty}^{\infty} e^{in\theta_{in}} \int_{\mathcal{S}} \int_0^{\bar{x}} \mathcal{A}^n(x_2, 0, \mathbf{s}_2) \, e^{-i\alpha x_2} \, dx_2 \, d\mathbf{s}_2^n, \tag{4.7}$$

$$\mathcal{N}_n(x, y) = x H_n'(x) J_n(y) - y H_n(x) J_n'(y) \tag{4.8}$$

and $\mathcal{X}_* = 0$, as we have assumed *hole correction* (3.17). For a more general pair distribution (3.19), we obtain

$$\mathcal{X}_* = \int_{a_{21} < R < \bar{a}_{21}} H_{n-m}(kR) J_{n-m}(k_* R) \chi(R \mid \mathbf{s}_1, \mathbf{s}_2) R \, dR, \tag{4.9}$$

where further details may be found in appendix Ba. We also remark that equation (4.5) reduces to ([5], eqn (87), [46], eqn (33)) for a single particle species.

To determine the effective wavenumber k_* we need only use (4.5). That is, the solution k_* is the one that leads to non-trivial solutions for the function $\mathcal{A}_*^m$. On the other hand, if $\mathcal{A}_*^m(\mathbf{s}_1)$ is a solution to (4.5), then so is $c\mathcal{A}_*^m(\mathbf{s}_1)$ for any constant c. To completely determine $\mathcal{A}_*^m(\mathbf{s}_1)$, we need to use (4.5) and (4.6).

Next, we determine closed-form estimates for k_* from (4.5) and determine the corresponding coefficients $\mathcal{A}_*^m(\mathbf{s}_1)$ for low number density in §7.

(a) Explicit expressions for k_* via expansions in the number density

We now consider the expansions

$$k_*^2 \sim K_{*0} + K_{*1}\mathfrak{n} + K_{*2}\mathfrak{n}^2 \quad \text{and} \quad \mathcal{A}_*^m \sim \mathcal{A}_{*0}^m + \mathcal{A}_{*1}^m\mathfrak{n} + \mathcal{A}_{*2}^m\mathfrak{n}^2, \tag{4.10}$$

where we use $\sim$ to denote an asymptotic expansion in $\mathfrak{n}$, which is formally equivalent to an expansion in volume fraction. We show in appendix Bb how substituting the above into equation (4.5) leads to

$$k_*^2 = k^2 - 4\mathfrak{n}\mathrm{i}\langle f_\circ\rangle(0) - 4\mathfrak{n}^2\mathrm{i}\langle f_{\circ\circ}\rangle(0) + \mathcal{O}(\mathfrak{n}^3), \tag{4.11}$$

where we assumed $K_{*0} = k^2$, though we deduce this in §7. Here we have

$$f_\circ(\theta, \mathbf{s}_1) = -\sum_{n=-\infty}^{\infty} \mathrm{e}^{\mathrm{i}n\theta} Z^n(\mathbf{s}_1) \quad \text{and} \quad \langle f_\circ\rangle(\theta) = -\sum_{n=-\infty}^{\infty} \mathrm{e}^{\mathrm{i}n\theta} \int_{\mathcal{S}} \mathrm{d}\mathbf{s}_1^n \tag{4.12}$$

and we introduce the multiple scattering pattern

$$\langle f_{\circ\circ}\rangle(\theta) = -\pi \sum_{n,m=-\infty}^{\infty} \int_{\mathcal{S}} \mathrm{e}^{\mathrm{i}n\theta} a_{12}^2 d_{n-m}(ka_{12}) \, \mathrm{d}\mathbf{s}_1^n \, \mathrm{d}\mathbf{s}_2^m, \tag{4.13}$$

where $\mathrm{d}\mathbf{s}_1^n = Z^n(\mathbf{s}_1)p(\mathbf{s}_1)\,\mathrm{d}\mathbf{s}_1$ and for convenience we define

$$d_m(x) = J_m'(x)H_m'(x) + \left(1 - \left(\frac{m}{x}\right)^2\right)J_m(x)H_m(x). \tag{4.14}$$

We remark that $f_\circ$ corresponds to the far-field scattering pattern for a single circular cylinder. This is evident by taking $N = 1$ in (2.11), which leads to

$$A_1^m = -\mathrm{i}^m \mathrm{e}^{-\mathrm{i}m\theta_{\mathrm{in}}} \mathrm{e}^{\mathrm{i}\mathbf{x}_1 \cdot \mathbf{k}} \tag{4.15}$$

and from (2.4) gives

$$\lim_{R_1 \to \infty} u_1 \sim \sqrt{\frac{2}{\pi k R_1}} f_\circ(\Theta_1 - \theta_{\mathrm{in}}, \mathbf{s}_1) \mathrm{e}^{\mathrm{i}kR_1 - \mathrm{i}\pi/4}.$$

We can interpret the terms on the right-hand side of (4.11) in the following way: the first k^2 corresponds to the incident wave, the second $4\mathfrak{n}\mathrm{i}\langle f_\circ\rangle(0)$ is the contribution from the incident wave scattered once from every cylinder (so-called 'single scattering') and the last $4\mathfrak{n}^2\mathrm{i}\langle f_{\circ\circ}\rangle(0)$ is the contribution of this scattered wave being re-scattered by every cylinder (so-called 'multiple scattering').

We can further specialize the wavenumber (4.11) by considering wavelengths $2\pi/k$ larger than the largest cylinder radius, or more precisely

$$ka_* := \max_{\mathbf{s}_1}\{ka_{11}p^2(\mathbf{s}_1)\} \ll 1, \tag{4.16}$$

which leads to

$$k_*^2 \sim k^2 - 4\mathfrak{n}\mathrm{i}\langle f_\circ\rangle(0) + \frac{8\mathfrak{n}^2}{\pi k^2}\int_0^\pi \cot\left(\frac{\theta}{2}\right)\frac{\mathrm{d}}{\mathrm{d}\theta}[\langle f_\circ\rangle(\theta)]^2 \, \mathrm{d}\theta + \mathcal{O}(k^4 a_*^4 \log(ka_*)), \tag{4.17}$$

where the integral converges because $\langle f_\circ\rangle'(0) = 0$. This expression and the derivation is analogous to that given in ([5], eqn (86)) for a single species. Although the sums in (4.11) converge quickly

for small ka_*, the form (4.17) is convenient as it is written in terms of the far-field scattering pattern $\langle f_\circ \rangle$.

An alternative approach [47] that is very useful in the context of low-frequency propagation is to take the quasi-static limit of the system (4.5). For small ka, the monopole and dipole scattering coefficients are both $O((ka)^2)$, which are the only contributions to the effective bulk modulus and density, respectively. Following the approach in [47], it is straightforward to show that for the N-species case, where the nth species has volume fraction ϕ_n, bulk modulus K_n and density ρ_n, the effective bulk modulus K_* and density ρ_* take the form

$$K_*^{-1} = K^{-1}(1-\phi) + \sum_{n=1}^{N} K_n^{-1}\phi_n \quad \text{and} \quad \rho_* = \rho\left(\frac{1 + \sum_{n=1}^{N} D_n\phi_n}{1 - \sum_{n=1}^{N} D_n\phi_n}\right), \tag{4.18}$$

where $\phi = \sum_n \phi_n$ and $D_n = (\rho_n - \rho)/(\rho_n + \rho)$.

Next, we explore how the expression (4.11) compares with other approaches by evaluating it numerically. In §7, we develop analytical expressions for the average scattering coefficient $\mathcal{A}^n$ and expressions for the reflection coefficient from the inhomogeneous halfspace.

5. Two species of cylinders

In this section, we analytically compare two approaches to calculating the effective wavenumber of a multi-species material. The first self-consistent type method homogenizes the small cylinder distribution and then determines effective properties for a large cylinder distribution embedded in the homogenized background, as shown in figure 2. The second determines the multi-species result using the approach outlined in previous sections.

(a) One small and one large species

We begin by assuming that there are only two species, S and L, that have constant wave speeds c_S and c_L, densities ρ_S and ρ_L, and number fractions $\mathfrak{n}_S$ and $\mathfrak{n}_L$, respectively. We assume that both types of cylinders have low volume fractions $\phi_S = \pi a_S^2 \mathfrak{n}_S$ and $\phi_L = \pi a_L^2 \mathfrak{n}_L$ and are proportional to one another $\phi_S \propto \phi_L$, so we will discard $O(\phi^3)$ terms, where $\phi = \phi_S + \phi_L$ denotes the total volume filling fraction. Note that it is more precise to assume small ϕ, rather than a small number density, since ϕ is non-dimensional.

First, the effective wavenumber k_{*S} of a material at long wavelengths with only a single species of S-cylinders is obtained by simplifying (4.17), where the far-field pattern (4.12) is, therefore, just the S cylinder species, i.e. there is no integral over $\mathbf{s}_1$ and $p(\mathbf{s}_1) = 1$. Assuming $c_S \neq 0$ and $\rho_S \neq 0$, we use ([8], eqn (24)) for small cylinder radius, which in our notation (recall $Z^n(\mathbf{s}_\ell) := Z_\ell^n$, where Z_ℓ^n is given in (2.5))

$$Z^0(\mathbf{s}_S) = i\pi \frac{a_S^2 k^2}{4} P + O(a_S^4) \quad \text{and} \quad Z^1(\mathbf{s}_S) = Z^{-1}(\mathbf{s}_S) = i\pi \frac{a_S^2 k^2}{4} Q + O(a_S^4), \tag{5.1}$$

where

$$P = 1 - \frac{k_S^2 \rho}{k^2 \rho_S} \quad \text{and} \quad Q = \frac{\rho - \rho_S}{\rho + \rho_S}. \tag{5.2}$$

Substituting the above into the simplified (4.17) leads to

$$\frac{k_{*S}}{k} = 1 - \frac{\phi_S}{2}(P + 2Q) - \frac{\phi_S^2}{8}(2P^2 - (P + 2Q)^2) + O(a_S^2) + O(\phi^3), \tag{5.3}$$

after taking a Taylor series for small $\mathfrak{n}$ for the square root. We also calculate the effective density ([8], eqn (1)) or refer to (4.18) with $N = 1$, given by

$$\frac{\rho_{*S}}{\rho} = \frac{\rho + \rho_S - \phi_S(\rho - \rho_S)}{\rho + \rho_S + \phi_S(\rho - \rho_S)} = 1 - 2\phi_S Q + O(a_S^2) + O(\phi^3), \tag{5.4}$$

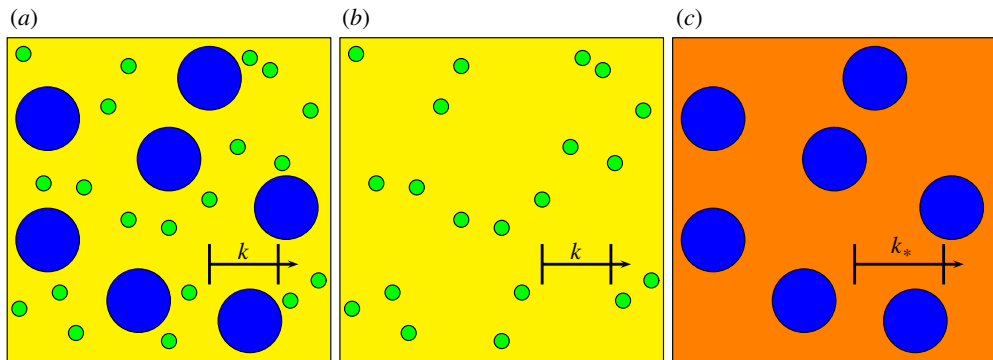which is appropriate for the approximation (5.3), see [8] for more details.

Figure 2. (a) Two-species material comprising large (blue) and small (green) inclusions in a background material (yellow) with incident wavenumber k, (b) one-species material comprising the small inclusions alone, and (c) one-species material with large cylinders alone in a background with incident wavenumber k_*, which is the effective wavenumber of (b). (Online version in colour.)

Next, we determine the effective wavenumber for large scatterers embedded in a background described by k_{*S} and ρ_{*S}. For this step, we introduce the notation $f_\circ(0, \mathbf{s}_1) = f_\circ(0, \mathbf{s}_1, \rho, k)$, which expresses the problem in terms of density and wavenumber in place of density and wave speed. Consequently, from (5.4), we have

$$f_\circ(0, \mathbf{s}_L, \rho_{*S}, k_{*S}) = f_{\circ L}(0) - \phi_S \delta f_{LS} + \mathcal{O}(a_S^2) + \mathcal{O}(\phi^2) \tag{5.5}$$

with

$$\delta f_{LS} := 2\rho Q \partial_\rho f_\circ(0, \mathbf{s}_L, \rho, k) + \frac{k}{2}(P + 2Q)\partial_k f_\circ(0, \mathbf{s}_L, \rho, k), \tag{5.6}$$

where we set $f_{\circ L}(0) := f_\circ(0, \mathbf{s}_L, \rho, k)$.

To calculate the wavenumber k_{*LS} for the L-cylinders in a material with a wavenumber k_{*S}, we use the formula (4.11) with k replaced by k_{*S}, $\langle f_\circ \rangle$ replaced with $f_\circ(0, \mathbf{s}_L, \rho_S^*, k_{*S})$ above and keeping only the integrands, that is, removing the integrals over the multi-species $\mathbf{s}_1$ and $\mathbf{s}_2$, to arrive at

$$k_{*LS}^2 = k_{*S}^2 + 4\mathrm{i}\frac{\phi_L^2}{\pi a_L^4} \sum_{n,p=-\infty}^{\infty} a_{LL}^2 d_{p-n}(k_{*S}a_{LL}) Z^n(\mathbf{s}_L, \rho_{*S}, k_{*S}) Z^p(\mathbf{s}_L, \rho_{*S}, k_{TS})$$

$$- \frac{4\mathrm{i}\phi_L}{\pi a_L^2} f_\circ(0, \mathbf{s}_L, \rho_{*S}, k_{*S}) + \mathcal{O}(\phi^3) \tag{5.7}$$

$$= k_{*S}^2 + 4\mathrm{i}\frac{\phi_L^2}{\pi a_L^4} \sum_{n,p=-\infty}^{\infty} a_{LL}^2 d_{p-n}(k a_{LL}) Z^n(\mathbf{s}_L, \rho, k) Z^p(\mathbf{s}_L, \rho, k)$$

$$- \frac{4\mathrm{i}\phi_L}{\pi a_L^2}(f_{\circ L}(0) - \phi_S \delta f_{LS}) + \mathcal{O}(a_S^2) + \mathcal{O}(\phi^3), \tag{5.8}$$

where we used $\mathrm{d}\mathbf{s}_j^m = Z^m(\mathbf{s}_j) p(\mathbf{s}_j) \, \mathrm{d}\mathbf{s}_j$. The above is an attempt to calculate the multi-species wavenumber by using only the single-species formula. However, the term of order $O(\phi_L \phi_S)$ in the above does not agree with (4.11), even in the limit $a_S \to 0$, as we show next.

For only two species of cylinders, and assuming the cylinders are uniformly distributed, the probability density function for the scattering properties becomes

$$p(\mathbf{s}) = \frac{\mathfrak{n}_S}{\mathfrak{n}} \delta(a - a_S)\delta(c - c_S)\delta(\rho - \rho_S) + \frac{\mathfrak{n}_L}{\mathfrak{n}} \delta(a - a_L)\delta(c - c_L)\delta(\rho - \rho_L), \tag{5.9}$$

which when substituted into (4.11) leads to the multi-species result

$$
k_*^2 = k^2 - 4i(n_S f_{\circ S}(0) + n_L f_{\circ L}(0)) + 4n_S^2 a_{SS}^2 \pi i \sum_{n,p=-\infty}^{\infty} d_{p-n}(k a_{SS}) Z^p(\mathbf{s}_S) Z^n(\mathbf{s}_S)
$$

$$
+ 8 n_S n_L a_{SL}^2 \pi i \sum_{n,p=-\infty}^{\infty} d_{p-n}(k a_{SL}) Z^p(\mathbf{s}_S) Z^n(\mathbf{s}_L)
$$

$$
+ 4 n_L^2 a_{LL}^2 \pi i \sum_{n,p=-\infty}^{\infty} d_{p-n}(k a_{LL}) Z^p(\mathbf{s}_L) Z^n(\mathbf{s}_L) + \mathcal{O}(\phi^3), \tag{5.10}
$$

where we used $a_{LS} = a_{SL}$. Assuming that $a_S \ll 1$ and using $a_{LS} = b_S + b_L$, with $b_S \geq a_S$ and $b_L \geq a_L$, we expand d_m (4.14) as

$$
d_m(k a_{SL}) = d_m(k b_L) + \frac{2 b_S}{b_L} [J_m(k b_L) H_m(k b_L) - d_m(k b_L)] + \mathcal{O}(a_S^2), \tag{5.11}
$$

where we use $b_S \propto a_S$. Substituting the above, (5.1), (5.3) and (5.8), into (5.10) we obtain

$$
k_*^2 = k_{*LS}^2 + \phi_L \phi_S \left[-\frac{4i}{\pi a_L^2} \delta f_{LS} + H_0 + \frac{a_S}{a_L} H_1 \right] + \mathcal{O}(a_S^2) + \mathcal{O}(\phi^3), \tag{5.12}
$$

where

$$
G_0 = \frac{8i}{\pi} \frac{b_L^2}{a_L^2} \sum_{n=-\infty}^{\infty} \sum_{p=-1}^{1} d_{p-n}(k b_L) \frac{Z^p(\mathbf{s}_S)}{a_S^2} Z^n(\mathbf{s}_L) \tag{5.13}
$$

and

$$
G_1 = \frac{16i}{\pi} \frac{b_L b_S}{a_L a_S} \sum_{n=-\infty}^{\infty} \sum_{p=-1}^{1} J_{p-n}(k b_L) H_{p-n}(k b_L) \frac{Z^p(\mathbf{s}_S)}{a_S^2} Z^n(\mathbf{s}_L). \tag{5.14}
$$

Note that $Z^p(\mathbf{s}_S)/a_S^2$ converges when $a_S \to 0$, see (5.1).

The terms in the brackets in (5.12) account for the interaction between the two types of cylinders, which is where the wavenumbers k_{*LS} (5.8) and k_* (5.12) differ. The leading-order error is non-vanishing even as the radius of the small species vanishes and is given by

$$
\lim_{a_S \to 0} \{k_* - k_{*LS}\} \approx \left(G_0 - \frac{4i}{\pi a_L^2} \delta f_{LS} \right) \phi_S \phi_L.
$$

A numerical investigation of this limit is conducted in §6. The physical meaning of these two terms are quite different: δf_{LS} is the change in the far-field scattering pattern of the L-cylinders due to changing the background wavenumber from k to k_{*S}, while G_0 accounts for the multiple scattering between the L and S-cylinders, which becomes significant when both ϕ_S are ϕ_L are large. Ultimately, this means that $k_* \approx k_{*LS}$ if either the S or L-cylinders are very dilute.

For comparison, we also give the two-dimensional version of eqn (23) of [28] given by

$$
k_{*C}^2 = k^2 - 4i n_S f_S(0) - 4i n_L f_L(0) + \frac{8 n_S^2}{\pi k^2} \int_0^{\pi} \cot(\theta/2) \frac{d}{d\theta} [f_S(\theta)]^2 \, d\theta
$$

$$
+ \frac{8 n_L^2}{\pi k^2} \int_0^{\pi} \cot(\theta/2) \frac{d}{d\theta} [f_L(\theta)]^2 \, d\theta \tag{5.15}
$$

and another commonly used approximation [48]

$$
k_{*0}^2 = k^2 - 4i n_S f_S(0) - 4i n_L f_L(0), \tag{5.16}
$$

describing the effective wavenumber for two species. However, the expression (5.15) is missing the interaction between the n_S and n_L species (the term $\mathcal{O}(n_S n_L)$) and is only valid for low frequency. Additionally, the estimate (5.16) ignores terms of the order $\mathcal{O}(\phi^2)$.

6. Numerical examples

In this section, we consider a selection of numerical examples to demonstrate the efficacy of (5.10) and other expressions. For k_{*LS}, we use the exact formula (4.11) for one species and then equation (5.7). This way, k_{*LS} is valid for S-cylinders with approximately zero density such as air. In the graphs that follow we use

$$\text{sound speed} = \frac{\omega}{\text{Re}\,k_*} \quad \text{and} \quad \text{attenuation} = \text{Im}\,k_*, \tag{6.1}$$

where k_* will be replaced with k_{*LS} and k_{*0} depending on the context.

For reference, we provide Julia [49] code to calculate the effective wavenumbers.

(a) Two-dimensional emulsion

Here we consider an emulsion composed of hexadecane (oil) and glycerol in water [50], table 2, where the glycerol forms very small inclusions. The graphs of figure 3a show how k_*, k_{*LS} and k_{*C} differ when varying only a_S the radius of the glycerol inclusions, for a fixed angular frequency $\omega = c/k_0 \approx 3 \times 10^6$ Hz. We observe that the difference between k_* and k_{*LS} persists even as $a_S \to 0$, as expected according to (5.12). Meaning that, no matter how small the S-cylinders become, the larger cylinders L do not perceive the S-cylinders as a homogeneous material, in the naive way described in §5a.

In fig. 21 of [28], they observed that experimentally measured wave speeds were shifted in comparison to the k_{*C} predictions, even for low-frequency. We can see this same discrepancy in figure 3b, where the angular frequency is varied between 1 KHz $< \omega < 12$ MHz while the radius $a_S = 25\,\mu$m is fixed. This discrepancy is due to the terms of order $O(\mathfrak{n}_L\mathfrak{n}_S)$ which are missing from k_{*C} (5.15) and k_{*LS} (5.10). Although all three wavenumbers are similar in figure 3b. The same is not true when we increase the frequency.

In figure 3c, we show how k_{*C}, valid only for low-frequency, strays from the more accurate k_* as the frequency increases,[1] where we did not include k_{*LS} as it is only valid for low frequency. There we can see that k_{*C} performs well up to about $ka_S = 0.3$, at which point $ka_L = 3.0$.

All the approximations k_{*0} (5.16), k_{*LS} (5.10) and k_{*C} (5.15) are missing second-order terms in the number density. In figure 4, we see the effect of these missing terms by varying the volume fraction while fixing $\omega = 3 \times 10^6$, or equivalently $ka_S = 0.5$. In the limit of low volume fraction, all three effective wavenumbers agree, as expected. For the largest volume fraction 40%, the expected error[2] of k_* is 6%. However, the relative difference between the attenuations of k_{*LS} and k_{*0} and the multi-species attenuation of k_* reaches 30%.

Summarizing figures 3 and 4, all the approximations are similar for either low frequency or low volume fraction. This is because the three phases in table 2 have similar properties. In our next example one of the phases, air, will be very different from the others, which will lead to more dramatic differences.
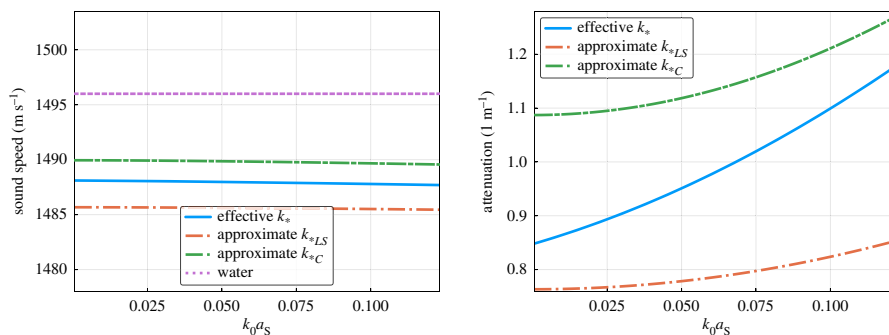
(b) Two-dimensional concrete

When there is a high contrast in the properties of the inclusions, multiple scattering can have a dramatic effect. To demonstrate this we consider a concrete-like material made from a limestone possessing cylinders of brick and air, given in table 3.

Figure 5 shows that it is only in the low-frequency limit, $ka_S < 0.05$, that the wavenumbers k_{*C} and k_{*LS} agree with the more exact k_*, which has a maximum expected relative error of only $\phi^3 = 0.16^3 \approx 0.4\%$. And in figure 5b, the wavenumber k_{*LS} appears to hit a resonance which should not

---

[1]In this case, we did not exactly use the two-dimensional version of eqn (23) from [28], but instead used a more accurate version where we summed enough terms for the far-field patterns to converge.

[2]If we disregard the error due to the low-frequency assumptions, we can estimate the expected errors $\phi^2 = 0.4^2 = 16\%$ for k_{*0} and $2\phi_L\phi_S = 2 * 0.2^2 = 8\%$ for both k_{*LS} and k_{*C}.

16

rspa.royalsocietypublishing.org   Proc. R. Soc. A **474**: 20170864

(a) fixed wavenumber $k = k_0$ while changing the radius a_S.

(b) fixed radius a_S while changing the wavenumber k
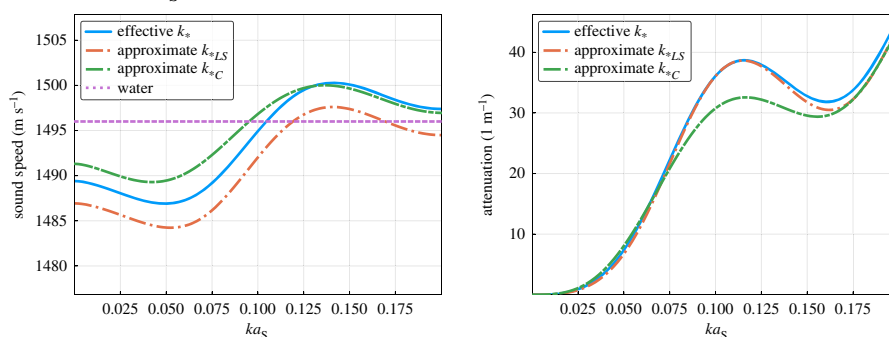
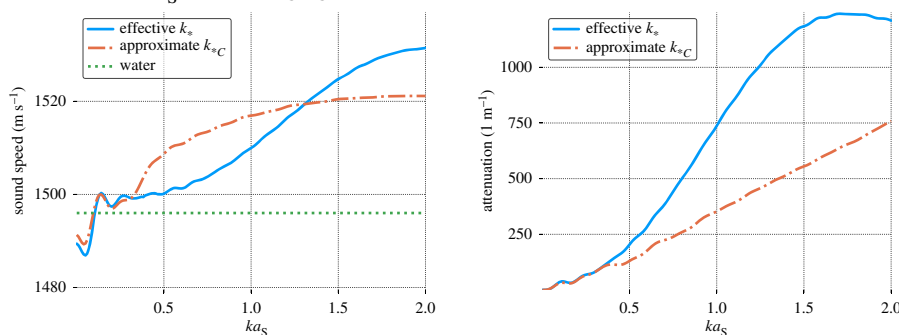(c) fixed radius a_S while changing the wavenumber k

Figure 3. Comparison of sound speeds and attenuation using wavenumbers k_{*C} (5.15), k_{*LS} (5.7), and k_* (5.10) for the water and oil emulsion from table 2. Code to generate figure: https://github.com/arturgower/EffectiveWaves.jl/tree/master/examples/emulsion. (a) Fixed wavenumber $k = k_0$ while changing the radius a_S, (b) fixed radius a_S while changing the wavenumber k and (c) fixed radius a_S while changing the wavenumber k. (Online version in colour.)

Table 2. Material properties used to approximate an emulsion.

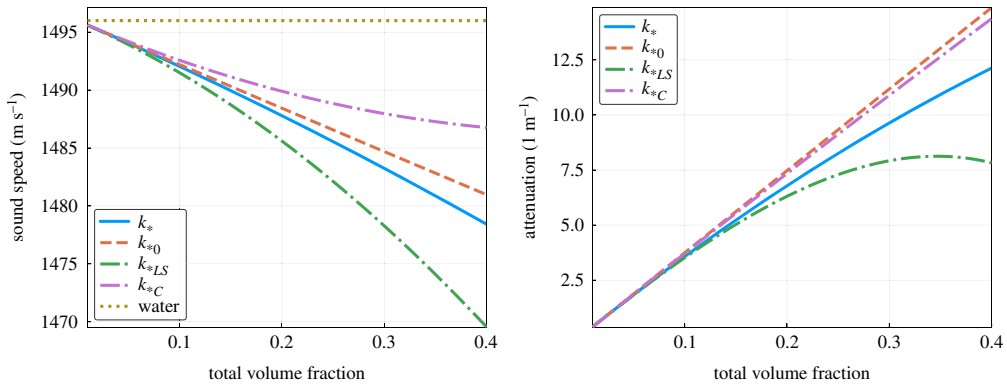|	density (kg m^{-3})	speed (m s^{-1})	radius (μm)	volume %
distilled water	$\rho = 998$	$c = 1496$	—	84%
hexadecane	$\rho_L = 773$	$c_L = 1338$	$a_L = 250$	$\phi_L = 11\%$
glycerol	$\rho_S = 1260$	$c_S = 1904$	$a_S = 25$	$\phi_S = 11\%$

Figure 4. Comparison of sound speeds and attenuation calculated from the effective wavenumbers k_{*C} (5.15), k_{*0} (5.16), k_{*LS} (5.7) and the more accurate k_* (5.10), as the total volume fraction of the inclusions increases (for the emulsion shown in table 2 with $ka_S = 0.5$). Code: https://github.com/arturgower/EffectiveWaves.jl/tree/master/examples/emulsion. (Online version in colour.)

Table 3. Material properties for our concrete-like material. Note that we used compacted limestone with very low porosity [51].

	density (kg m^{-3})	speed (m s^{-1})	radius (mm)	volume %
limestone	$\rho = 2460$	$c = 4855$	—	84%
brick	$\rho_l = 1800$	$c_l = 3650$	$a_l = 2.0$	$\phi_l = 10\%$
dry air	$\rho_S = 1.293$	$c_S = 331.4$	$a_S = 0.2$	$\phi_S = 6\%$

be present. This, and the dramatic changes in attenuation at low frequency, are expected because for an inclusion with low density, the effective wavenumber diverges for fixed volume fraction when k tends to zero [8]. Figure 5c shows the limitations of k_{*C} as the frequency increases. Even though k_{*C} is only valid for low frequencies, its results are quite close to k_*, having a relative difference of around 25%.

Again as expected, all the wavenumbers converge as the volume fraction decreases (figure 6), yet the differences in the wave speed are significant, reaching 100% in this example, when the total volume fraction $\phi = 40\%$.

7. The average field and reflection

In this section, we determine the reflected field from a halfspace, which is achieved by deducing the averaged scattering coefficient $\mathcal{A}^n$, for low number density shown in (4.10)$_2$.

In order to calculate $\mathcal{A}^n$ we first use (4.6) and (4.11), except here we can deduce that $K_{*0} = k^2$. As θ_* appears in (4.6), we expand

$$\theta_* = \theta_{*0} + \theta_{*1}\mathfrak{n} + \theta_{*2}\mathfrak{n}^2 + \mathcal{O}(\mathfrak{n}^2), \tag{7.1}$$

which combined with Snell's equation (4.4) and the number density expansions (4.10) gives for the first two orders:

$$K_{*0}\sin(\theta_{*0})^2 = k^2\sin(\theta_{in})^2, \quad k^2\theta_{*1}\cos(\theta_{*0}) = 2\mathrm{i}\langle f_\circ\rangle(0)\frac{\sin(\theta_{*0})^3}{\sin(\theta_{in})^2}. \tag{7.2}$$
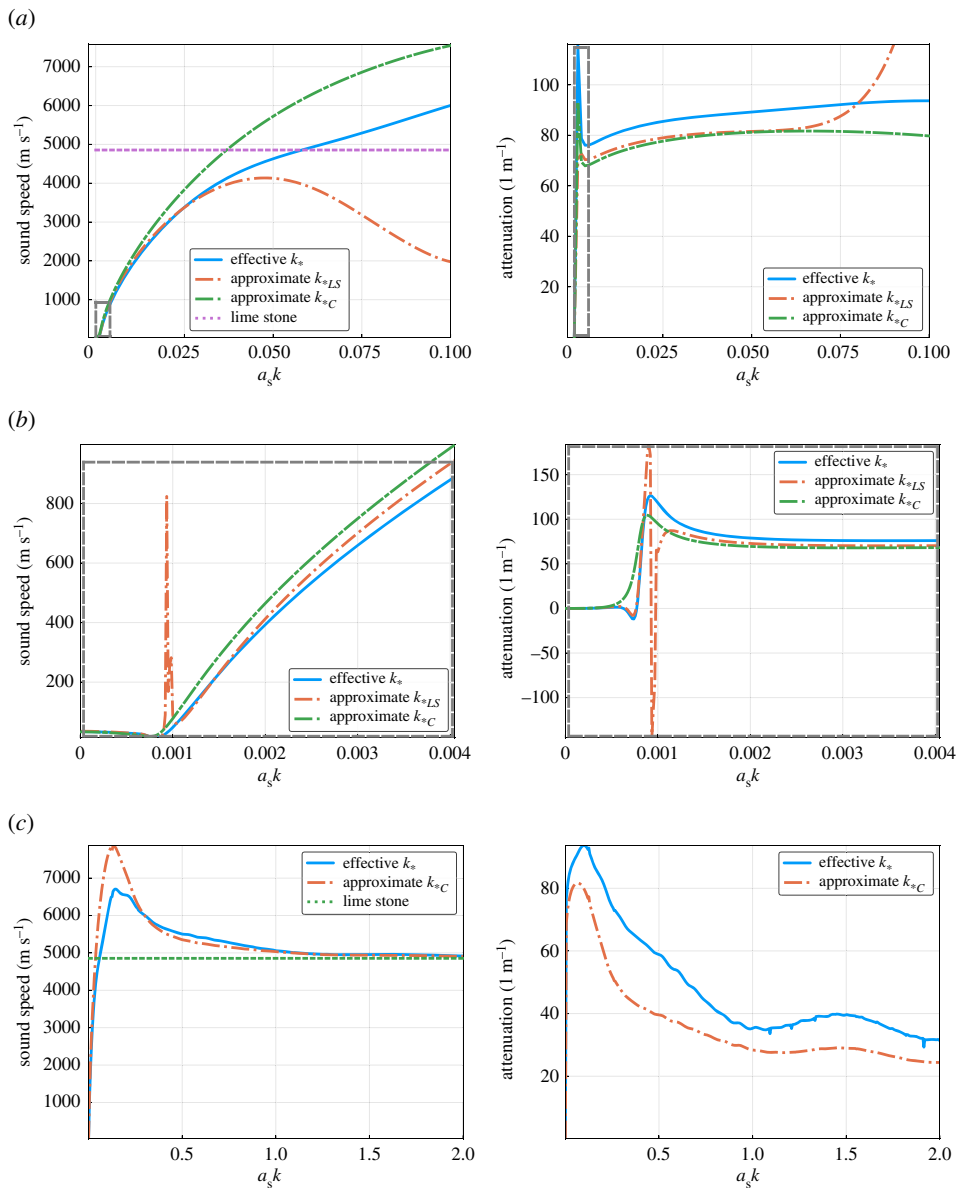
(*a*)

(*b*)

(*c*)

Figure 5. Sound speed and attenuation from the approximate wavenumbers k_{*C} (5.15) and k_{*LS} (5.7) with the more accurate k_* (5.10) for the concrete-like mixture shown in table 3. Code: https://github.com/arturgower/EffectiveWaves.jl/tree/master/examples/concrete. (*a*) Fixed wavenumber $k = k_0$ while changing the radius a_S, (*b*) same as (*a*) but for smaller $a_S k$ and (*c*) fixed radius a_S while changing the wavenumber k. (Online version in colour.)

For $\bar{x}$, which appears in equation (4.6), we assume that, as $\mathfrak{n} \to 0$, $\bar{x}$ is a fixed width large enough for the effective wave ansatz (4.3) to hold, meaning that

$$\bar{x} = \mathcal{O}(1), \quad \int_0^{\bar{x}} \mathcal{A}^n(x_2, \mathbf{s}) \, e^{-i\alpha x_2} \, dx_2 = \mathcal{O}(1). \tag{7.3}$$

Using the above in (4.6) we conclude that $K_{*0} = k^2$, to ensure that $\mathfrak{n}^{-1}$ appears on the left-hand side. Subsequently, using $K_{*0} = k^2$ in (7.2) leads to

$$\theta_{*0} = \theta_{\text{in}}, \quad \theta_{*1} = \frac{2i\langle f_\circ \rangle(0)}{k^2} \tan \theta_{\text{in}} \tag{7.4}$$
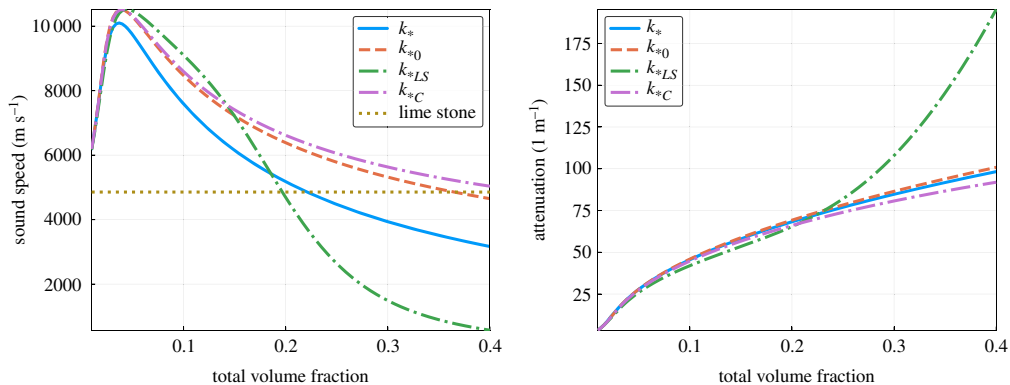
19

rspa.royalsocietypublishing.org *Proc. R. Soc. A* **474**: 20170864

Figure 6. Sound speed and attenuation from the three effective wavenumbers k_{*C} (5.15), k_{*0} (5.16) and k_{*LS} (5.7), with the more accurate k_* (5.10), against the total volume fraction of the inclusions for the concrete shown in table 3. (Online version in colour.)

and

$$\theta_{*2} = \theta_{*1}^2 \left[\frac{\cos\theta_{\text{in}}}{\sin\theta_{\text{in}}} + \frac{1}{\sin(2\theta_{\text{in}})} \right] + 2\mathrm{i}\frac{\langle f_{\circ\circ}\rangle(0)}{k^2}\tan\theta_{\text{in}}, \tag{7.5}$$

where θ_{*2} is given for completeness. We use the above to expand

$$\frac{\mathrm{e}^{\mathrm{i}(\alpha_* - \alpha)\bar{x}}}{\alpha_* - \alpha} = \mathrm{i}\bar{x} + \left[\frac{1}{\mathfrak{n}} - \frac{\langle f_{\circ\circ}\rangle(0)}{\langle f_{\circ}\rangle(0)} \right] \frac{\mathrm{i}k}{2\langle f_{\circ}\rangle(0)}\cos\theta_{\text{in}} + \frac{1}{2k}\sec\theta_{\text{in}} + \mathcal{O}(\mathfrak{n}), \tag{7.6}$$

then we substitute the leading order term in the above into (4.6) leading to: $\langle f_{\circ}\rangle(0) = \sum_{n=-\infty}^{\infty}\int_S \mathcal{A}_{*0}^n\,\mathrm{d}\mathbf{s}_2^n$. However, from (B 13) we found that $\mathcal{A}_{*0}^n$ is independent of n and $\mathbf{s}_2$, therefore, $\mathcal{A}_{*0}^n = -1$. This means that $\mathcal{A}_*^n$ tends, in the limit $\mathfrak{n} \to 0$, to the scattering coefficient of one lone cylinder:

$$\mathcal{A}^m(\mathbf{x}_1,\mathbf{s}_1) \to \mathrm{i}^m \mathcal{A}_{*0}^m(\mathbf{s}_1)\,\mathrm{e}^{-\mathrm{i}m\theta_{*0}}\,\mathrm{e}^{\mathrm{i}x_1\cdot\sqrt{K_{*0}}} = -\mathrm{i}^m\,\mathrm{e}^{-\mathrm{i}m\theta_{\text{in}}}\,\mathrm{e}^{\mathrm{i}\mathbf{x}_1\cdot\mathbf{k}} = A_1^m, \tag{7.7}$$

where we used $K_{*0} = k^2$ and $\theta_{*0} = \theta_{\text{in}}$, and the last equation is from (4.15).

To calculate the next order in $\mathfrak{n}$ of equation (4.6) we need to calculate $b(\bar{x})$. To do so, we assume that $\mathcal{A}^n(\mathbf{x}_2,\mathbf{s}_2) \to A_2^n$ as $\mathfrak{n} \to 0$ for every $x_2 > 0$. That is, in the limit where there are no cylinders, except one fixed at $\mathbf{x}_2$, the averaged scattering coefficient $\mathcal{A}^n$ tends to the scattering coefficient of one lone cylinder, even for $0 < x_2 < \bar{x}$. As a result

$$\mathcal{A}^n(x_2,0,\mathbf{s}_2) = -\mathrm{i}^n\,\mathrm{e}^{-\mathrm{i}n\theta_{\text{in}}}\,\mathrm{e}^{\mathrm{i}\alpha x_2} + \mathcal{O}(\mathfrak{n}), \quad \text{for } x_2 > 0,$$

which when substituted in $b(\bar{x})$ from (4.6), together with (4.12), leads to $b(\bar{x}) = \mathrm{i}\bar{x}\langle f_{\circ}\rangle(0) + \mathcal{O}(\mathfrak{n})$. Substituting this, (7.6), and (7.5) into (4.6), and then ignoring second-order terms $\mathcal{O}(\mathfrak{n}^2)$ we obtain

$$\frac{-\mathrm{i}\langle f_{\circ\circ}\rangle(0)k\cos\theta_{\text{in}}}{2\langle f_{\circ}\rangle(0)} + \frac{\mathrm{i}k\cos\theta_{\text{in}}}{2\langle f_{\circ}\rangle(0)}\sum_{n=-\infty}^{\infty}\int_S \mathcal{A}_{*1}^n(\mathbf{s}_2)\,\mathrm{d}\mathbf{s}_2^n = -\frac{\langle f_{\circ}\rangle(0)}{2k\cos\theta_{\text{in}}} + \mathcal{O}(\mathfrak{n}^2), \tag{7.8}$$

where we also used $\sum_{n=-\infty}^{\infty}\int_S n\,\mathrm{d}\mathbf{s}_2^n = 0$, which is a result of the property $Z_2^n = Z_2^{-n}$, see (2.5), implying that $\mathrm{d}\mathbf{s}_2^n = \mathrm{d}\mathbf{s}_2^{-n}$. In appendix Bb, we showed that the quantity F_*, given by (B 16), is independent of n and $\mathbf{s}_2$. So if we substitute $\mathcal{A}_{*1}^n(\mathbf{s}_2)$ for F_*, we can then take F_* outside the sum and integral in (7.8), and then substitute back $\mathcal{A}_{*1}^n(\mathbf{s}_2)$ to arrive at

$$\mathcal{A}_{*1}^n(\mathbf{s}_2) = -\frac{\mathrm{i}\langle f_{\circ}\rangle(0)}{k^2\cos^2\theta_{\text{in}}} - \pi\sum_{m=-\infty}^{\infty}\int_S a_{12}^2 d_{m-n}(ka_{12})\,\mathrm{d}\mathbf{s}_1^m + \mathcal{O}(\mathfrak{n}^2), \tag{7.9}$$

where we used (4.12)$_2$. The above reduces to the one-species case given in ([52], eqn (27)). With $\mathcal{A}_{*1}^n$ and $\mathcal{A}_{*0}^n$, we can now calculate reflection from a halfspace.
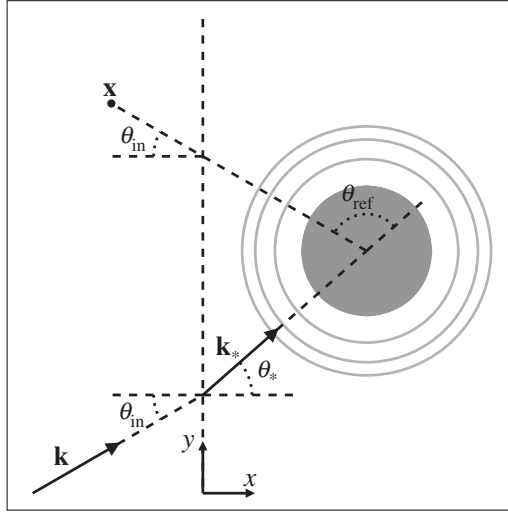
Figure 7. The far-field reflected angle θ_{ref}, where $\mathbf{k} = (\alpha, \beta)$ and $\mathbf{k}_*$ is the effective transmitted wavenumber defined in §4. The wavenumber $\mathbf{k}_*$ results from ensemble averaging all scattered waves originating from $x > 0$ (to the right of the dashed vertical line). The reflected field measured at $\mathbf{x}$ can be understood as the scattering (the grey circles) of the transmitted wave by an effective particle (grey particle). In the figure, θ_{ref} equals $\pi - \theta_* - \theta_{\mathrm{in}}$, but for small number density $\theta_* = \theta_{\mathrm{in}} + \mathcal{O}(\mathfrak{n})$, which is why $\theta_{\mathrm{ref}} = \pi - 2\theta_{\mathrm{in}}$ appears in (1.3) and (1.4).

(a) Reflection from a halfspace

Here we calculate the reflected wave measured at (x, y), where $x < 0$. To achieve this, we assume that the boundary layer around $x = 0$ has little effect on the reflected wave, that is, we assume most of the scatterers behave as if they are in an infinite medium. This is the same as taking $\bar{x} = 0$, which was also used in [52], where they showed that this approach matches other homogenization results in the low-frequency limit. We note, however, that Felbacq et al. [53] discuss the possibility of a boundary layer effect even in the low-frequency limit.

Substituting (3.9) into the total effective wave (3.8), and using the form (4.3) reveals

$$\langle u(x, y) \rangle = \mathrm{e}^{\mathrm{i}\mathbf{k}\cdot\mathbf{x}} + \mathfrak{n}\,\mathrm{e}^{-\mathrm{i}m\theta_*} \sum_{m=-\infty}^{\infty} \mathrm{i}^m \int_{\mathcal{S}} \mathcal{A}_*^m(\mathbf{s}_1) \int_{0 < x_1 < \infty} \mathrm{e}^{\mathrm{i}\beta y_1 + \mathrm{i}\alpha_* x_1} \Phi_m(kR_1, \Theta_1)\,\mathrm{d}x_1\,\mathrm{d}\mathbf{s}_1^m, \qquad (7.10)$$

where we used $u_{\mathrm{in}}(x, y) = \mathrm{e}^{\mathrm{i}\mathbf{k}\cdot\mathbf{x}}$, $\mathrm{d}\mathbf{s}_1^m = Z_1^m p(\mathbf{s}_1)\,\mathrm{d}\mathbf{s}_1$, $\Phi_m(kR_1, \Theta_1) = H_m^{(1)}(kR_1)\,\mathrm{e}^{\mathrm{i}m\Theta_1}$, substituted (3.14), used $N = |\mathcal{R}_N|\mathfrak{n}$ and took the limit $N \to \infty$. Then using (B 5) and (B 7), we obtain

$$\int_{0 < x_1 < \infty} \mathrm{e}^{\mathrm{i}\beta y_1 + \mathrm{i}\alpha_* x_1} \Phi_m(kR_1, \Theta_1)\,\mathrm{d}x_1 = \mathrm{e}^{-\mathrm{i}\alpha x + \mathrm{i}\beta y} \frac{2}{\alpha} \frac{(-\mathrm{i})^{-m}\mathrm{i}}{\alpha + \alpha_*} \mathrm{e}^{-\mathrm{i}m\theta_{\mathrm{in}}}, \qquad (7.11)$$

noting that $x_1 - x > 0$. Using the above in (7.10), we reach

$$\langle u(x, y) \rangle = \mathrm{e}^{\mathrm{i}\mathbf{k}\cdot\mathbf{x}} + \frac{2\mathfrak{n}}{\alpha} \frac{\mathrm{i}\,\mathrm{e}^{-\mathrm{i}\alpha x + \mathrm{i}\beta y}}{\alpha + \alpha_*} \sum_{m=-\infty}^{\infty} \mathrm{e}^{\mathrm{i}m\theta_{\mathrm{ref}}} \int_{\mathcal{S}} \mathcal{A}_*^m(\mathbf{s}_1)\,\mathrm{d}\mathbf{s}_1^m, \qquad (7.12)$$

where $\theta_{\mathrm{ref}} = \pi - \theta_* - \theta_{\mathrm{in}}$. The reflected wave shown by (1.2) is calculated by expanding for small $\mathfrak{n}$, including $\theta_{\mathrm{ref}} = \pi - 2\theta_{\mathrm{in}} + \mathcal{O}(\mathfrak{n})$, and then substituting the results from §7. For a single-species this formula reduces to ([52], eqn (41) and (42)). Figure 7 gives a pictorial representation of the reflection coefficient in (7.12).

8. Conclusion

We have deduced the effective wavenumbers (1.1) and (1.5), and reflection coefficient (1.2), for a multi-species material up to moderate number density and over a broad range of frequencies. This will enable experimental researchers to extract more information about the makeup of inhomogeneous media (see the electronic supplementary material for self-contained expressions for the wavenumbers and reflection coefficients in the case of a finite number of species). We also remark that the results may be extended straightforwardly to multiple scattering from cylinders in a number of contexts, including two-dimensional electromagnetism.

Characterization is not the only application; this theory can also be employed to design novel materials. We have shown that multiple scattering between different species can lead to effective properties that are not exhibited by single-species media. That is, using our multi-species formulae it is now possible to choose species so as to design impedance matched, highly dispersive and broad band attenuating materials.

We also saw that the multi-species effective wavenumbers derived in the acoustics literature were accurate for low frequency and low volume fraction. But to go beyond these limitations, our more precise effective wavenumber was needed. We also illustrated that a 'self-consistent' approach to calculating the effective wavenumber is not even accurate at low frequencies.

Two main issues of our method deserve further investigation: the effects of the boundary layer near the surface of the halfspace and the QCA. To calculate the reflection coefficient up to second order in the number density, we neglected the effects of the boundary layer. It is not clear how to theoretically make progress without these two approximations, nor what errors they introduce. We believe that these issues represent important future work.

Appendix A. Effective wavenumber for multi-species spherical inclusions

In this section, we apply our multi-species theory to the results in [21] for spherical inclusions to reach the effective wavenumber (1.5). Details are omitted when the results follow by direct analogy. For spheres we define the ensemble-average far-field pattern and multiple scattering pattern,

$$\langle F_\circ \rangle(\theta) = -\sum_{n=0}^{\infty} P_n(\cos\theta) \int_{\mathcal{S}} (2n+1)\, \mathrm{d}\mathbf{s}_1^n \tag{A 1}$$

and

$$\langle F_{\circ\circ} \rangle = \frac{\mathrm{i}(4\pi)^2}{2} \sum_{n=0}^{\infty} \sum_{p=0}^{\infty} \sum_{q} \int_{\mathcal{S}} \int_{\mathcal{S}} \frac{\sqrt{(2n+1)(2p+1)}}{(4\pi)^{3/2}}$$

$$\sqrt{2q+1}\, \mathcal{G}(n,0;p,0;q) k a_{12} D_q(k a_{12})\, \mathrm{d}\mathbf{s}_1^n\, \mathrm{d}\mathbf{s}_2^p, \tag{A 2}$$

where q takes the values

$$|n-p|, |n-p|+2, |n-p|+4, \ldots, n+p,$$

$\mathrm{d}\mathbf{s}_i^n = \zeta^n(\mathbf{s}_i)p(\mathbf{s}_i)\,\mathrm{d}\mathbf{s}_i$, $D_m(x) = xj_m'(x)(xh_m'(x) + h_m(x)) + (x^2 - m(m+1))j_m(x)j_m(x)$, P_n are Legendre polynomials, j_m are spherical Bessel functions, h_m are spherical Hankel functions of the first kind and

$$\zeta^m(\mathbf{s}_j) = \frac{q_j j_m'(ka_j)j_m(k_j a_j) - j_m(ka_j)j_m'(k_j a_j)}{q_j h_m'(ka_j)j_m(k_j a_j) - h_m(ka_j)j_m'(k_j a_j)} = \zeta^{-m}(\mathbf{s}_j), \tag{A 3}$$

with $q_j = (\rho_j c_j)/(\rho c)$, where $\mathcal{G}$ is a Gaunt coefficient ([21], eqn (A.5)) defined here as

$$\mathcal{G}(n, 0; p, 0; q) = \frac{\sqrt{(2n+1)(2p+1)(2q+1)}}{2\sqrt{4\pi}} \int_0^\pi P_n(\cos\theta)P_p(\cos\theta)P_q(\cos\theta)\sin\theta\,\mathrm{d}\theta. \tag{A 4}$$

Appendix B. Calculating the effective equations (4.6) and (4.5)

In this appendix, we provide an in-depth outline of the derivation for (4.6) and (4.5), which are given in terms of the unknowns $\mathcal{A}^n(\mathbf{x}_2, \mathbf{s})$ and k_*. The approach here is similar to Section IV in [5].

We begin by substituting (4.1) and (4.3) into the integral in the governing equation (3.24) which for $x_1 > \bar{x} + a_{21}$ takes the form

$$\int_{\substack{x_2 > 0 \\ R_{21} > a_{21}}} \mathcal{A}^n(\mathbf{x}_2, \mathbf{s})\Phi_{n-m}(kR_{21}, \Theta_{21})\,\mathrm{d}\mathbf{x}_2$$

$$= \mathrm{e}^{\mathrm{i}\beta y_1}\,\mathrm{e}^{-\mathrm{i}(n-m)\pi} \int_0^{\bar{x}} \mathcal{A}^n(x_2, 0, \mathbf{s})L_{n-m}(x_2 - x_1)\,\mathrm{d}x_2$$

$$+ \mathrm{i}^n\,\mathrm{e}^{-\mathrm{i}n\theta_*}\,\mathrm{e}^{-\mathrm{i}(n-m)\pi}\,\mathcal{A}_*^n\,\mathrm{e}^{\mathrm{i}\mathbf{k}_*\cdot\mathbf{x}_1} \int_{\substack{X > \bar{x} - x_1 \\ R > a_{21}}} \mathrm{e}^{\mathrm{i}\mathbf{k}_*\cdot\mathbf{X}}\Phi_{n-m}(kR, \Theta)\,\mathrm{d}\mathbf{X}, \tag{B 1}$$

where $X = x_2 - x_1$ and $Y = y_2 - y_1$, so that (R, Θ) are the polar coordinates of $\mathbf{X} = (X, Y)$, where $R = R_{21}$ and $\Theta = \Theta_{21} - \pi$, and we define

$$\Phi_{n-m}(kR, \Theta) := \mathrm{e}^{\mathrm{i}(n-m)\Theta}H_{n-m}(kR), \quad L_{n-m}(X) := \int_{-\infty}^\infty \mathrm{e}^{\mathrm{i}\beta Y}\Phi_{n-m}(kR, \Theta)\,\mathrm{d}Y. \tag{B 2}$$

From eqn (37) of [52], we have

$$L_n(X) = \begin{cases} \dfrac{2}{\alpha}(-\mathrm{i})^n\,\mathrm{e}^{-\mathrm{i}n\theta_{\mathrm{in}}}\,\mathrm{e}^{\mathrm{i}\alpha X}, & \text{for } X > 0, \\[2ex] \dfrac{2}{\alpha}\mathrm{i}^n\,\mathrm{e}^{\mathrm{i}n\theta_{\mathrm{in}}}\,\mathrm{e}^{-\mathrm{i}\alpha X}, & \text{for } X < 0. \end{cases} \tag{B 3}$$

To calculate the last integral in (B 1), it is necessary that $k_* \neq k$, as $k_* = k$ leads to a divergent integrand. Assuming $k_* \neq k$, we observe that

$$\mathrm{e}^{\mathrm{i}\mathbf{k}_*\cdot\mathbf{X}}\Phi_{n-m}(kR, \Theta) = \frac{1}{k^2 - k_*^2}[\Phi_{n-m}(kR, \Theta)\nabla^2\,\mathrm{e}^{\mathrm{i}\mathbf{k}_*\cdot\mathbf{X}} - \mathrm{e}^{\mathrm{i}\mathbf{k}_*\cdot\mathbf{X}}\nabla^2\Phi_{n-m}(kR, \Theta)]$$

because $\nabla^2\Phi_{n-m}(kR, \Theta) = -k^2\Phi_{n-m}(kR, \Theta)$ and $\nabla^2\,\mathrm{e}^{\mathrm{i}\mathbf{k}_*\cdot\mathbf{X}} = -k_*^2\,\mathrm{e}^{\mathrm{i}\mathbf{k}_*\cdot\mathbf{X}}$. Then by Green's second identity, we obtain

$$\int_{\substack{X > \bar{x} - x_1 \\ R > a_{21}}}[\Phi_{n-m}(kR, \Theta)\nabla^2\,\mathrm{e}^{\mathrm{i}\mathbf{k}_*\cdot\mathbf{X}} - \mathrm{e}^{\mathrm{i}\mathbf{k}_*\cdot\mathbf{X}}\nabla^2\Phi_{n-m}(kR, \Theta)]\,\mathrm{d}\mathbf{X}$$

$$= \int_{\partial\mathcal{B}}\left[\Phi_{n-m}(kR, \Theta)\frac{\partial\,\mathrm{e}^{\mathrm{i}\mathbf{k}_*\cdot\mathbf{X}}}{\partial\mathbf{n}} - \mathrm{e}^{\mathrm{i}\mathbf{k}_*\cdot\mathbf{x}}\frac{\partial\Phi_{n-m}(kR, \Theta)}{\partial\mathbf{n}}\right]\,\mathrm{d}s, \tag{B 4}$$

where $\mathbf{n}$ is the outwards pointing unit normal. For $x_1 > a_{21}$, the region $\mathcal{B}$ is given by $X > \bar{x} - x_1$ and $R > a_{21}$, so that the boundary $\partial\mathcal{B}$ is the circle $R = a_{21}$ and the line $X = \bar{x} - x_1$. The integral on the left-hand side of (B 4) reduces to the form

$$\int_{\mathcal{B}} e^{i\mathbf{k}_* \cdot \mathbf{X}} \Phi_{n-m}(kR, \Theta) \, d\mathbf{X} = \frac{1}{\alpha^2 - \alpha_*^2}(M_\circ + M_-), \tag{B 5}$$

where $k^2 - k_*^2 = \alpha^2 - \alpha_*^2$. Here, we have [5, eqn (68)]:

$$M_\circ = 2\pi i^{n-m} e^{i(n-m)\theta_*} \mathcal{N}_{n-m}(ka_{12}, k_* a_{12}), \tag{B 6}$$

where $\mathcal{N}_{n-m}$ is defined by (4.8), and

$$M_- = -\int_{-\infty}^{\infty} \left[\Phi_{n-m}(kR, \Theta) \frac{\partial e^{i\mathbf{k}_* \cdot \mathbf{X}}}{\partial X} - e^{i\mathbf{k}_* \cdot \mathbf{X}} \frac{\partial \Phi_{n-m}(kR, \Theta)}{\partial X} \right] dY$$

$$= \begin{cases} 2\dfrac{\alpha_* + \alpha}{\alpha} i^{n-m-1} e^{i(\alpha_* - \alpha)X} e^{i(n-m)\theta_{\text{in}}}, & \text{for } X < 0, \\[3mm] 2\dfrac{\alpha_* - \alpha}{\alpha} i^{-(n-m)-1} e^{i(\alpha_* + \alpha)X} e^{-i(n-m)\theta_{\text{in}}}, & \text{for } X > 0, \end{cases} \tag{B 7}$$

for $X = \bar{x} - x_1 < 0$, which is identical to ([5], eqn (67)) (with the replacements $\ell \mapsto \bar{x}$ and $\lambda \mapsto \alpha_*$, and where we have included the case $X > 0$ for future reference).

From (B 5), it follows that (B 1) now becomes

$$\int_{\substack{x_2 > 0 \\ R_{21} > a_{21}}} \mathcal{A}^n(\mathbf{x}_2, \mathbf{s}) \Phi_{n-m}(kR_{21}, \Theta_{21}) \, d\mathbf{x}_2 = i^m e^{i\beta y_1} [e^{-im\theta_*} e^{i\alpha_* x_1} \mathcal{B}^{n,m} + e^{i\alpha x_1} e^{i(n-m)\theta_{\text{in}}} \mathcal{C}^{n,m}],$$

where

$$\mathcal{B}^{n,m} = \mathcal{A}_*^n \frac{2\pi}{k^2 - k_*^2} \mathcal{N}_{n-m}(ka_{12}, k_* a_{12}) \tag{B 8}$$

and

$$\mathcal{C}^{n,m} = \frac{2}{\alpha} \int_0^{\bar{x}} (-i)^n \mathcal{A}^n(x_2, 0, \mathbf{s}) e^{-i\alpha x_2} \, dx_2 + \frac{2}{\alpha} i \mathcal{A}_*^n e^{-in\theta_*} \frac{e^{i(\alpha_* - \alpha)\bar{x}}}{\alpha_* - \alpha}. \tag{B 9}$$

Substituting the above into (3.24), assuming $x_1 > \bar{x} + a_{21}$, and cancelling common factors, we arrive at

$$e^{i\alpha_* x_1} e^{-im\theta_*} \left[\mathcal{A}_*^m + \mathfrak{n} \sum_{n=-\infty}^{\infty} \int_{\mathcal{S}} \mathcal{B}^{n,m} \, d\mathbf{s}_2^n \right] + e^{i\alpha x_1} e^{-im\theta_{\text{in}}} \left[\mathfrak{n} \sum_{n=-\infty}^{\infty} e^{in\theta_{\text{in}}} \int_{\mathcal{S}} \mathcal{C}^{n,m} \, d\mathbf{s}_2^n + 1 \right] = 0, \tag{B 10}$$

having also used $I_1 = e^{i(\alpha_* x_1 + \beta y_1)}$. As the above must hold for all x_1, we can equate the terms in the brackets to zero, which leads to (4.6) and (4.5).

(a) Effective wave for any pair distribution

To calculate the effective wave for any pair distribution function χ satisfying (3.21), we substitute (3.19) into (3.24), which leads to an extra integral appearing on the left side of (B 1):

$$\int_{\substack{\mathcal{R}_\infty \\ R_{21} > a_{21}}} \mathcal{A}^n(\mathbf{x}_2, \mathbf{s}_2) \Phi_{n-m}(kR_{21}, \Theta_{21}) \chi(R_{21}|\mathbf{s}_1, \mathbf{s}_2) \, d\mathbf{x}_2$$

$$= i^n \mathcal{A}_*^n(\mathbf{s}_2) e^{-in\theta_*} e^{-i(n-m)\pi} e^{i\mathbf{k}_* \cdot \mathbf{x}_1} \int_{\substack{X > \bar{x} - x_1 \\ a_{21} < R < \bar{a}_{21}}} e^{i\mathbf{k}_* \cdot \mathbf{X}} \Phi_{n-m}(kR, \Theta) \chi(R|\mathbf{s}_1, \mathbf{s}_2) \, d\mathbf{X}$$

$$+ e^{-i(n-m)\pi} \int_{\substack{-x_1 \leq X \leq \bar{x} - x_1 \\ a_{21} < R < \bar{a}_{21}}} \mathcal{A}^n(\mathbf{x}_2, \mathbf{s}_2) \Phi_{n-m}(kR, \Theta) \chi(R|\mathbf{s}_1, \mathbf{s}_2) \, d\mathbf{x}_2,$$

where $X = x_2 - x_1$ and $Y = y_2 - y_1$, so that (R, Θ) are the polar coordinates of $\mathbf{X} = (X, Y)$, where $R = R_{21}$, $\Theta = \Theta_{21} - \pi$. The second integral on the right is zero when $x_1 > \bar{x} + \bar{a}_{21}$ because then

$$-x_1 \leq X \leq \bar{x} - x_1 < -\bar{a}_{21}$$

and $\mathbf{X}$ can not satisfy both $X < -\bar{a}_{21}$ and $a_{21} < R < \bar{a}_{21}$.

24

rspa.royalsocietypublishing.org   *Proc. R. Soc. A* **474**: 20170864

For $x_1 > \bar{x} + \bar{a}_{21}$, the integral over the regions $X > \bar{x} - x_1$ and $a_{21} < R < \bar{a}_{21}$ reduces to the just $a_{21} < R < \bar{a}_{21}$, so leaving out the factors on the left, and using $e^{i\mathbf{k}_* \cdot \mathbf{X}} = e^{ik_* R \cos(\Theta - \theta_*)}$, the integral becomes

$$\int_{a_{21} < R < \bar{a}_{21}} \int_0^{2\pi} e^{ik_* R \cos(\Theta - \theta_*)} e^{i(n-m)\Theta} H_{n-m}(kR) \chi(R \mid \mathbf{s}_1, \mathbf{s}_2) R \, d\Theta \, dR,$$

$$= 2\pi i^{n-m} e^{i(n-m)\theta_*} \mathcal{X}_*, \tag{B 11}$$

where we used the Jacobi–Anger expansion and $\mathcal{X}_*$ is defined by (4.9). In conclusion, we should sum $2\pi \mathcal{A}_*^n(\mathbf{s}_2)\mathcal{X}_*$ to $\mathcal{B}_{n,m}$, appearing in equations (B 8) and (B 10).

(b) Low number fraction

To calculate k_*^2 we need only equation (4.5), which after substituting (4.10) and

$$\mathcal{N}_m(ka_{12}, k_* a_{12}) \sim \frac{2i}{\pi} + \mathfrak{n} K_{*1} \frac{a_{21}^2}{2} d_m(ka_{21}), \tag{B 12}$$

with d_m defined by (4.14), and then equating terms of order $\mathcal{O}(1)$ and $\mathcal{O}(\mathfrak{n})$, leads to

$$\mathcal{A}_{*0}^m(\mathbf{s}_1) = \frac{4i}{K_{*1}} \sum_{n=-\infty}^{\infty} \int_{\mathcal{S}} \mathcal{A}_{*0}^n(\mathbf{s}_2) \, d\mathbf{s}_2^n \tag{B 13}$$

and

$$\mathcal{A}_{*1}^m(\mathbf{s}_1) - \pi \sum_{n=-\infty}^{\infty} \int_{\mathcal{S}} a_{21}^2 d_{n-m}(ka_{21}) \mathcal{A}_{*0}^n(\mathbf{s}_2) \, d\mathbf{s}_2^n$$

$$= \frac{4i}{K_{*1}} \sum_{n=-\infty}^{\infty} \int_{\mathcal{S}} \left[\mathcal{A}_{*1}^n(\mathbf{s}_2) - \mathcal{A}_{*0}^n(\mathbf{s}_2) \frac{K_{*2}}{K_{*1}} \right] d\mathbf{s}_2^n. \tag{B 14}$$

Turning to (B 13), we see that $\mathcal{A}_{*0}^m(\mathbf{s}_1)$ is independent of both m and $\mathbf{s}_1$. Let $\mathcal{A}_{*0} := \mathcal{A}_{*0}^n(\mathbf{s}_2) = \mathcal{A}_{*0}^m(\mathbf{s}_1)$, then we can divide both sides of (B 13) by $\mathcal{A}_{*0}$ (assuming $\mathcal{A}_{*0} \neq 0$), and use (4.12) to arrive at

$$K_{*1} = -4i\langle f_\circ \rangle(0). \tag{B 15}$$

Turning to (B 14), we see that

$$F_* = \mathcal{A}_{*1}^m(\mathbf{s}_1) - \pi \mathcal{A}_{*0} \sum_{n=-\infty}^{\infty} \int_{\mathcal{S}} a_{21}^2 \, d_{n-m}(ka_{21}) \, d\mathbf{s}_2^n \tag{B 16}$$

is independent of both m and $\mathbf{s}_1$, which we use to write (B 14) as

$$F_* = -\frac{1}{\langle f_\circ \rangle(0)} \sum_{n=-\infty}^{\infty} \int_{\mathcal{S}} \mathcal{A}_{*1}^n(\mathbf{s}_2) \, d\mathbf{s}_2^n - i\mathcal{A}_{*0} \frac{K_{*2}}{4\langle f_\circ \rangle(0)}$$

$$= -\frac{F_*}{\langle f_\circ \rangle(0)} \sum_{n=-\infty}^{\infty} \int_{\mathcal{S}} d\mathbf{s}_2^n - i\mathcal{A}_{*0} \frac{K_{*2}}{4\langle f_\circ \rangle(0)} + \mathcal{A}_{*0} \frac{\langle f_{\circ\circ} \rangle(0)}{\langle f_\circ \rangle(0)},$$

where we used (4.13). This simplifies to $K_{*2} = -4i\langle f_{\circ\circ} \rangle(0)$, which together with (B 15), (4.10) leads to the effective wavenumber (4.11).

References

1. Pinfield VJ, Challis RE. 2013 Emergence of the coherent reflected field for a single realisation of spherical scatterer locations in a solid matrix. *J. Phys. Conf. Ser.* **457**, 012009. (doi:10.1088/1742-6596/457/1/012009)
2. Foldy LL. 1945 The multiple scattering of waves. I. General theory of isotropic scattering by randomly distributed scatterers. *Phys. Rev.* **67**, 107. (doi:10.1103/PhysRev.67.107)

3. Tsang L, Ishimaru A. 1987 Radiative wave equations for vector electromagnetic propagation in dense nontenuous media. *J. Electromagn. Waves Appl.* **1**, 59–72. (doi:10.1163/156939387X00090)

4. Tsang L, Chen CT, Chang ATC, Guo J, Ding KH. 2000 Dense media radiative transfer theory based on quasicrystalline approximation with applications to passive microwave remote sensing of snow. *Radio Sci.* **35**, 731–749. (doi:10.1029/1999RS002270)

5. Linton CM, Martin PA. 2005 Multiple scattering by random configurations of circular cylinders: second-order corrections for the effective wavenumber. *J. Acoust. Soc. Am.* **117**, 3413–3423. (doi:10.1121/1.1904270)

6. Lax M. 1951 Multiple scattering of waves. *Rev. Mod. Phys.* **23**, 287–310. (doi:10.1103/RevModPhys.23.287)

7. Martin PA, Maurel A. 2008 Multiple scattering by random configurations of circular cylinders: weak scattering without closure assumptions. *Wave Motion* **45**, 865–880. (doi:10.1016/j.wavemoti.2008.03.004)

8. Martin PA, Maurel A, Parnell WJ. 2010 Estimating the dynamic effective mass density of random composites. *J. Acoust. Soc. Am.* **128**, 571–577. (doi:10.1121/1.3458849)

9. Chekroun M, Le Marrec L, Lombard B, Piraux J. 2012 Time-domain numerical simulations of multiple scattering to extract elastic effective wavenumbers. *Waves Random Complex Media* **22**, 398–422. (doi:10.1080/17455030.2012.704432)

10. West R, Gibbs D, Tsang L, Fung AK. 1994 Comparison of optical scattering experiments and the quasi-crystalline approximation for dense media. *J. Opt. Soc. Am. A* **11**, 1854–1858. (doi:10.1364/JOSAA.11.001854)

11. Lax M. 1952 Multiple scattering of waves. II. The effective field in dense systems. *Phys. Rev.* **85**, 621. (doi:10.1103/PhysRev.85.621)

12. Waterman PC. 1971 Symmetry, unitarity, and geometry in electromagnetic scattering. *Phys. Rev. D.* **3**, 825–839. (doi:10.1103/PhysRevD.3.825)

13. Varadan VK, Varadan VV, Pao YH. 1978 Multiple scattering of elastic waves by cylinders of arbitrary cross section. I. SH waves. *J. Acoust. Soc. Am.* **63**, 1310–1319. (doi:10.1121/1.381883)

14. Mishchenko MI, Travis LD, Mackowski DW. 1996 T-matrix computations of light scattering by nonspherical particles: a review. *J. Quant. Spectrosc. Radiat. Transf.* **55**, 535–575. (doi:10.1016/0022-4073(96)00002-7)

15. Ding KH, Tsang L. 1988 Effective propagation constants of dense nontenuous media with multi-species of particles. *J. Electromagn. Waves Appl.* **2**, 757–777.

16. Tedesco M, Kim EJ. 2006 Intercomparison of electromagnetic models for passive microwave remote sensing of snow. *IEEE. Trans. Geosci. Remote Sens.* **44**, 2654–2666. (doi:10.1109/TGRS.2006.873182)

17. Tourin A, Fink M, Derode A. 2000 Multiple scattering of sound. *Waves Random Media* **10**, R31–R60. (doi:10.1088/0959-7174/10/4/201)

18. Sheng P. 2006 *Introduction to wave scattering, localization and mesoscopic phenomena*, vol. 88. Berlin, Germany: Springer Science & Business Media.

19. Martin P. 2003 Acoustic scattering by inhomogeneous obstacles. *SIAM. J. Appl. Math.* **64**, 297–308. (doi:10.1137/S0036139902414379)

20. Fikioris JG, Waterman PC. 1964 Multiple scattering of waves. II. 'Hole corrections' in the scalar case. *J. Math. Phys.* **5**, 1413–1420. (doi:10.1063/1.1704077)

21. Linton CM, Martin PA. 2006 Multiple scattering by multiple spheres: a new proof of the Lloyd–Berry formula for the effective wavenumber. *SIAM. J. Appl. Math.* **66**, 1649–1668. (doi:10.1137/050636401)

22. Spelt PDM, Norato MA, Sangani AS, Greenwood MS, Tavlarides LL. 2001 Attenuation of sound in concentrated suspensions: theory and experiments. *J. Fluid Mech.* **430**, 51–86. Cambridge. (doi:10.1017/S002211200000272X)

23. Spelt PDM, Norato MA, Sangani AS, Tavlarides LL. 1999 Determination of particle size distributions from acoustic wave propagation measurements. *Phys. Fluids* **11**, 1065–1080. (doi:10.1063/1.869977)

24. Baudoin M, Thomas JL, Coulouvrat F, Lhuillier D. 2007 An extended coupled phase theory for the sound propagation in polydisperse concentrated suspensions of rigid particles. *J. Acoust. Soc. Am.* **121**, 3386–3397. (doi:10.1121/1.2723648)

25. Waterman PC, Truell R. 1961 Multiple scattering of waves. *J. Math. Phys.* **2**, 512–537.

26. Van der Meulen F, Feuillard G, Bou Matar O, Levassort F, Lethiecq M. 2001 Theoretical and experimental study of the influence of the particle size distribution on acoustic

26

rspa.royalsocietypublishing.org *Proc. R. Soc. A* **474**: 20170864

wave properties of strongly inhomogeneous media. *J. Acoust. Soc. Am.* **110**, 2301–2307. (doi:10.1121/1.1404435)

27. Javanaud C, Gladwell NR, Gouldby SJ, Hibberd DJ, Thomas A, Robins MM. 1991 Experimental and theoretical values of the ultrasonic properties of dispersions: effect of particle state and size distribution. *Ultrasonics* **29**, 331–337. (doi:10.1016/0041-624X(91)90031-3)

28. Challis RE, Povey MJW, Mather ML, Holmes AK. 2005 Ultrasound techniques for characterizing colloidal dispersions. *Rep. Prog. Phys.* **68**, 1541–1637. (doi:10.1088/0034-4885/68/7/R01)

29. Lloyd P, Berry MV. 1967 Wave propagation through an assembly of spheres: IV. Relations between different multiple scattering theories. *Proc. Phys. Soc.* **91**, 678–688. (doi:10.1088/0370-1328/91/3/321)

30. Caleap M, Drinkwater BW, Wilcox PD. 2012 Effective dynamic constitutive parameters of acoustic metamaterials with random microstructure. *New. J. Phys.* **14**, 033014. (doi:10.1088/1367-2630/14/3/033014)

31. Gower AL. 2017 EffectiveWaves.jl: a package to calculate the effective waves travelling in materials comprised of randomly distributed particles or inclusions. See https://github.com/arturgower/EffectiveWaves.jl.

32. Sabina FJ, Willis JR. 1988 A simple self-consistent analysis of wave propagation in particulate composites. *Wave Motion* **10**, 127–142. (doi:10.1016/0165-2125(88)90038-8)

33. Yang RB. 2003 A dynamic generalized self-consistent model for wave propagation in particulate composites. *J. Appl. Mech.* **70**, 575–582. (doi:10.1115/1.1576806)

34. Kim JY. 2004 On the generalized self-consistent model for elastic wave propagation in composite materials. *Int. J. Solids Struct.* **41**, 4349–4360. (doi:10.1016/j.ijsolstr.2004.03.020)

35. Gajdardziska-Josifovska M, McPhedran RC, McKenzie DR, Collins RE. 1989 Silver–magnesium fluoride cermet films. 2: optical and electrical properties. *Appl. Opt.* **28**, 2744–2753. (doi:10.1364/AO.28.002744)

36. Linton CM, McIver P. 2001 *Handbook of mathematical techniques for wave/structure interactions*. London, UK: Chapman and Hall.

37. Martin PA. 2006 *Multiple scattering: interaction of time-harmonic waves with N obstacles*, vol. 107. Cambridge, UK: Cambridge University Press.

38. Abramowitz M, Stegun IA. 1966 *Handbook of mathematical functions: with formulas, graphs, and mathematical tables*. Applied mathematics series, vol. 55. North Chelmsford, MA: Courier Corporation.

39. Pinfield VJ, Challis RE. 2012 Simulation of incoherent and coherent backscattered wave fields from cavities in a solid matrix. *J. Acoust. Soc. Am.* **132**, 3760–3769. (doi:10.1121/1.4763985)

40. Parnell WJ, Abrahams ID, Brazier-Smith PR. 2010 Effective properties of a composite half-space: exploring the relationship between homogenization and multiple-scattering theories. *Q. J. Mech. Appl. Math.* **63**, 145–175. (doi:10.1093/qjmam/hbq002)

41. Caleap M, Drinkwater BW, Wilcox PD. 2012 Coherent acoustic wave propagation in media with pair-correlated spheres. *J. Acoust. Soc. Am.* **131**, 2036–2047. (doi:10.1121/1.3675011)

42. Bose SK. 1996 Ultrasonic plane SH wave reflection from a uni-directional fibrous composite slab. *J. Sound Vib.* **193**, 1069–1078. (doi:10.1006/jsvi.1996.0332)

43. Twersky V. 1978 Acoustic bulk parameters in distributions of pair-correlated scatterers. *J. Acoust. Soc. Am.* **64**, 1710–1719. (doi:10.1121/1.382150)

44. Ding KH, Mandt CE, Tsang L, Kong JA. 1992 Monte Carlo simulations of pair distribution functions of dense discrete random media with multiple sizes of particles. *J. Electromagn. Waves Appl.* **6**, 1015–1030.

45. Bose SK, Mal AK. 1974 Elastic waves in a fiber-reinforced composite. *J. Mech. Phys. Solids* **22**, 217–229. (doi:10.1016/0022-5096(74)90026-X)

46. Bose SK, Mal AK. 1973 Longitudinal shear waves in a fiber-reinforced composite. *Int. J. Solids Struct.* **9**, 1075–1085. (doi:10.1016/0020-7683(73)90016-4)

47. Parnell WJ, Abrahams ID. 2010 Multiple point scattering to determine the effective wavenumber and effective material properties of an inhomogeneous slab. *Waves Random Complex Media* **20**, 678–701. (doi:10.1080/17455030.2010.510858)

48. Ma Y, Varadan VK, Varadan VV. 1984 Application of Twersky's multiple scattering formalism to a dense suspension of elastic particles in water. *J. Acoust. Soc. Am.* **75**, 335–339. (doi:10.1121/1.390476)

27

rspa.royalsocietypublishing.org *Proc. R. Soc. A* **474**: 20170864

49. Bezanson J, Edelman A, Karpinski S, Shah V. 2017 Julia: a fresh approach to numerical computing. *SIAM Rev.* **59**, 65–98. (doi:10.1137/141000671)
50. Magdassi S, Frank SG. 1986 Formation of oil-in-glycerol/water emulsions. *J. Dispers. Sci. Technol.* **7**, 599–612.
51. Parent T, Domede N, Sellier A, Mouatt L. 2015 Mechanical characterization of limestone from sound velocity measurement. *Int. J. Rock Mech. Mining Sci.* **79**, 149–156. (doi:10.1016/j.ijrmms.2015.08.009)
52. Martin PA. 2011 Multiple scattering by random configurations of circular cylinders: Reflection, transmission, and effective interface conditions. *J. Acoust. Soc. Am.* **129**, 1685–1695. (doi:10.1121/1.3546098)
53. Felbacq D, Tayeb G, Maystre D. 1994 Scattering by a random set of parallel cylinders. *J. Opt. Soc. Am. A* **11**, 2526–2538. (doi:10.1364/JOSAA.11.002526)